frontiers | Frontiers in Earth Science

ORIGINAL RESEARCH
published: 03 June 2022
doi: 10.3389/feart.2022.897882

Structural Characteristics and Deformation Evolution of an Intra-Continental Fold-Thrust Belt in Eastern Sichuan: Insights Into Analogue Sandbox Models

Yang-Shuang Wang[1], *Mo Xu*[1]*, *Yan-Na Yang*[1], *Qiang Xia*[1], *Bing Jiang*[1], *Chang Yang*[2] *and Heng Zhang*[3]

[1]State Key Laboratory of Geohazard Prevention and Geoenvironment Protection, College of Environment and Civil Engineering, Chengdu University of Technology, Chengdu, China, [2]Chongqing Institute of Geology and Mineral Resources, Chongqing, China, [3]Sichuan Metallurgical Geological Survey and Design Group Co. Ltd, Chengdu, China

OPEN ACCESS

Edited by:
Xiaoyan Zhao,
Southwest Jiaotong University, China

Reviewed by:
Hua-Wen Cao,
China Geological Survey, China
Deng Mingzhe,
SINOPEC Petroleum Exploration and Production Research Institute, China

***Correspondence:**
Mo Xu
xm@cdut.edu.cn

Specialty section:
This article was submitted to Geohazards and Georisks, a section of the journal Frontiers in Earth Science

Received: *16 March 2022*
Accepted: *22 April 2022*
Published: *03 June 2022*

Citation:
Wang Y-S, Xu M, Yang Y-N, Xia Q, Jiang B, Yang C and Zhang H (2022) Structural Characteristics and Deformation Evolution of an Intra-Continental Fold-Thrust Belt in Eastern Sichuan: Insights Into Analogue Sandbox Models. Front. Earth Sci. 10:897882. doi: 10.3389/feart.2022.897882

The Eastern Sichuan area is a typical fold-and-impulse zone. It is bounded by the Qiyue Mountain fault, with septal folds on the east and on the west. Based on previous geological mapping and surface geological structure research as well as the fault-related folding theory, in this study, tectonophysical simulation experiments were conducted to investigate the tectonic geometry and kinematics of the Eastern Sichuan fold-impulse zone. The experiments were conducted by selecting different experimental materials and changing the physical properties of the cover, the friction between the cover and the basement, the number of slip layers, the burial depth, and other factors. Finally, the similarity of the results to the morphological characteristics of the real geological structure was assessed. The results show that the deformation style is influenced to some extent by the brittle shear strength and the ductile shear strength of the basement, and the different interlayer cohesions between the competent and incompetent layers, the high rheology, and the burial depth of the slickensides played crucial roles in the formation of the final evolution of the Eastern Sichuan fold fault zone. The step-like system, composed of a lower crustal crystalline basement detachment surface, regional boundary fractures, and the overlying Cambrian and Triassic synclines, is a necessary condition for the formation of the Eastern Sichuan fold and fault zone and controls the overall evolution of the zone. Under the action of multiple phases of tectonic activity with different main stress orientations, the geological phenomenon of multiple superimposed phases of folding in different directions observed at present in the Eastern Sichuan area was formed. The well-developed karst features are not conducive to the construction of a project tunnel in the area where tightly closed back-slope, fissures, and normal faults have developed in the Eastern Sichuan fold and fault zone.

Keywords: Eastern Sichuan, physical simulation, slippage, folded-splash zones, tectonic geometry, and kinematics, engineering influence

1 INTRODUCTION

The concept of a fold and thrust belt was introduced by Rich (1934) for the first time. Since then, many scholars have conducted relevant research on this topic. In general, the terms "thick-skinned" and "thin-skinned" tectonics are widely used when describing the structural geometry of fold and thrust belts (Pfiffner 2006). Thick-skinned tectonics involves thrust faults that reach down into the crystalline basement. In some cases, the thrust faults run parallel to the basement cover contact a few kilometers beneath this contact. In contrast, thin-skinned tectonics relates to thrust sheets where the sedimentary cover is detached from its crystalline substratum along a detachment layer that consists of mechanically weak rocks. The thickness of the detached cover sediments is typically in the order of 1–10 km (Adrian 2017). Understanding the styles of deformation processes and the mechanisms of faulting and folding is crucial, all of which are active in variable proportions throughout the entire evolution of a fold and thrust belt (Jamison 1992; Woodward 1999). Understanding both the interactions and the relationship between the macroscopic fold and thrust processes and the mesoscopic and microscopic fabric-forming processes is necessary to reconstruct the tectonic evolution.

As one of the typical tectonic styles of fold and thrust belts in the foreland region of a collisional zone, the Eastern Sichuan fold-thrust belt (ESFTB) is situated in the eastern margin of the middle and upper Yangtze blocks in the South China Craton (Charvet 2013; Lu et al., 2014; Zhang et al., 2013) (**Figure 1**). It is bordered by the Dabashan arcuate thrust belt to the northeast, the Youjiang fold-thrust belt to the south, the Xuefeng–Dayong fold-thrust belt to the east, and the Huayingshan fault to the west (Tang and Cui 2012; Zhao et al., 2017). In a similar way, the ESFTB consists of two deformation domains with significantly different deformation styles and characteristics (Li et al., 2015). The Western Hunan–Hubei thick-skinned tectonic zone located between the Qiyueshan and Dayong faults is characterized by trough-like folds, while the Eastern Sichuan thin-skinned tectonic zone located between the Qiyueshan and Huayingshan faults is characterized by a high-steep anticline (**Figure 2**). Therefore, the ESFTB is an ideal area to study Jura-type folds.

Recent research and geological exploration have confirmed that in such systems, a weak basal layer (e.g., gypsum and shale) serves as the main décollement, which has been recognized as a key factor controlling the deformation of the sedimentary sequences during shortening (Davis and Terry 1985; Oner and Dilek 2013; Mount 2014; Boutoux et al., 2016). Two or multiple layer detachments have been reported in many folds and thrust belts worldwide, such as the Jura fold-thrust belt in Switzerland (Rameil 2008; Malz et al., 2016), the Apennines in Italy (Massoli et al., 2006; Tavani and Cifelli 2010), the southeast Zagros in Iran (Ghazian and Buiter 2014), and the Western Gibraltar Arc between the Mediterranean and the Atlantic (Expósito et al., 2012). Based on the statistics of drilling holes, field investigations, and seismic dates, the ESFTB was mainly controlled by two ductile décollements: 1) one in the gypsum and shale of the Lower–Middle Cambrian Longwangmiao Formation and Gaotai Formation and 2) the other in the dark gray gypsum-bearing dolomite of the Lower Triassic Jialingjiang Formation. However, although previous research has consistently concluded that these detachments played an important role in the development and deformation progress of the ESFTB (Chu et al., 2012a; Tang and Cui 2012; Li et al., 2015), few studies have been conducted on the relationship between the deformation processes, the mechanisms of the folding and thrusting, and the mechanical properties, relative thickness, depth, and vertical and horizontal distribution of the multiple décollements (Brogi 2008; Hayes and Hanks 2008). Furthermore, the structural characteristics and geodynamic origin of the ESFTB are still debated, and the proposed tectonic interpretations vary (Li et al., 2002; Yan et al., 2003; Shen et al., 2009; Li 2015; Zou et al., 2015).

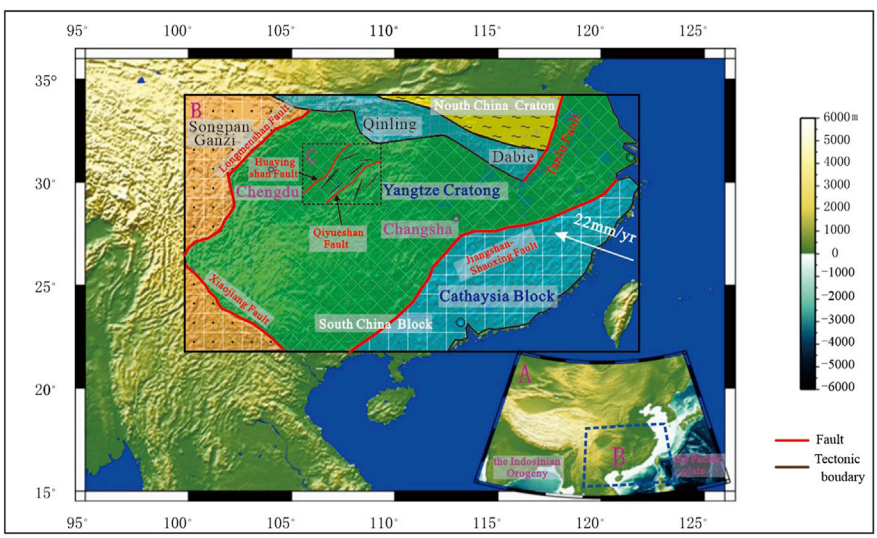

FIGURE 1 | Tectonic map of South China (modified after Deng et al., 2014).

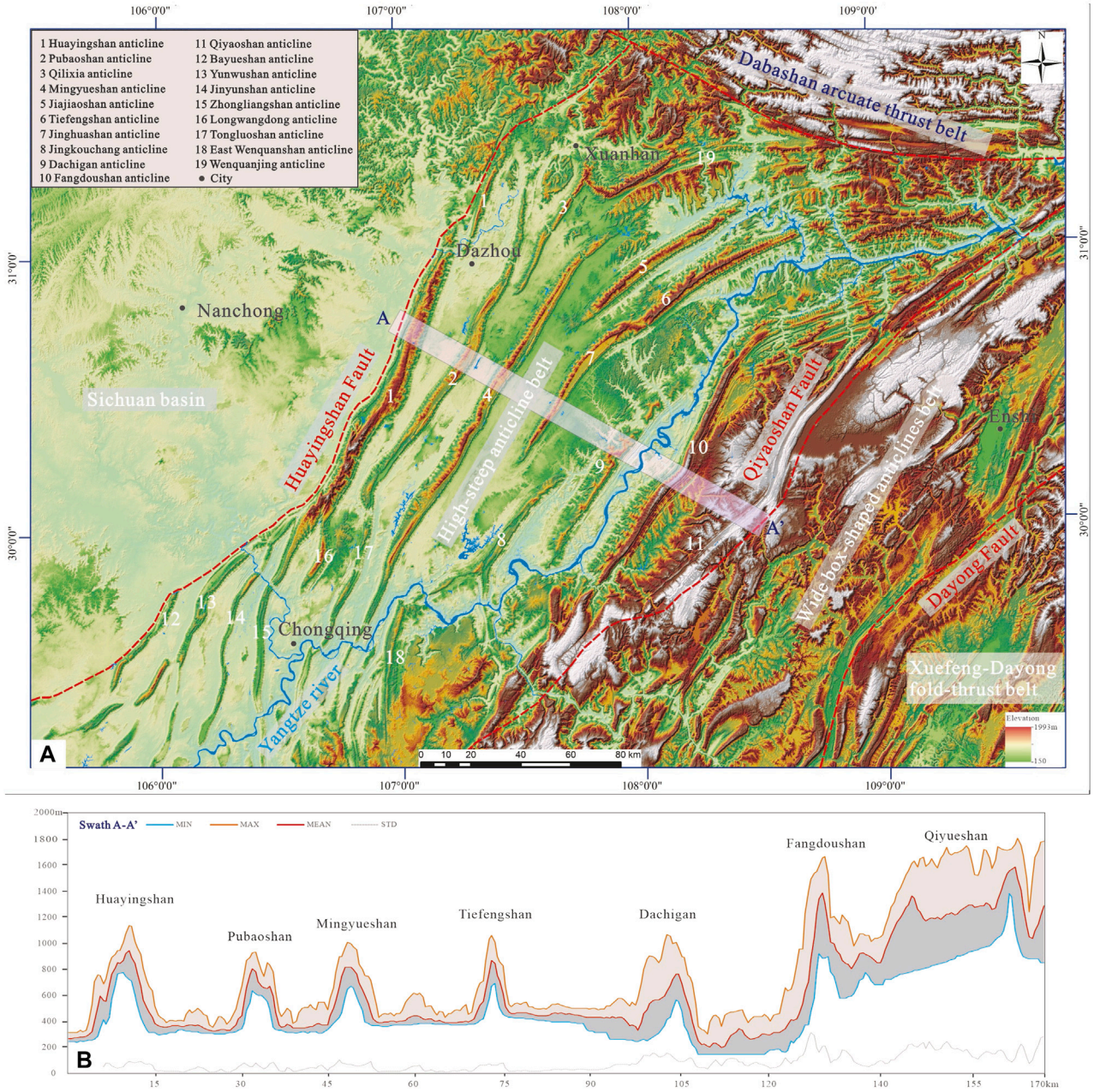

FIGURE 2 | Location and digital elevation map of the study area. **(A)** Digital elevation map of the Eastern Sichuan basin (on **Figure 1** for location). **(B)** Cross section of the digital elevation map of the Eastern Sichuan basin (See A–A′ on **(A)** for location).

Physical analog modeling has been proven to be an effective tool for studying the deformation processes and mechanisms of fold and thrust belts (Zanon and Janette Souza Gomes 2019; Meng and Hodgetts 2019; Graveleau et al., 2012; Santolaria et al., 2015; Santolaria et al., 2015). Previous studies have revealed that many factors play important roles in the analog modeling of fold and thrust belts, such as the physical properties of the materials, the rate of shortening, the thickness ratio of the brittle overburden to the basal décollement, and the geometry and dip of the boundaries (Rossetti et al., 2000; Bonini et al., 2012; Reiter et al., 2011). In this study, six sets of analog modeling experiments were conducted to systematically investigate the geometry and timing of the deformation progress, as well as how and where the shortening was accommodated. Each experiment was analyzed based on detailed monitoring, field geological surveys, digital elevation model (DEM) measurements, and seismic sections. Finally, based on existing research results and the results of this study, the structural

deformation was comprehensively analyzed, providing new robust insights into the tectonic evolution of the ESFTB.

2 GEOLOGIC SETTING AND PETROGRAPHY

2.1 Background Geology of the Yangtze Block in the South China Craton

The ESFTB was controlled by the evolution of the middle and upper Yangtze blocks in the South China Craton (SCC), which have experienced a complex tectonic evolution since the early Neoproterozoic (**Figure 1A**) (Charvet 2013; Lu et al., 2014; Deng et al., 2014). The basement of the Yangtze Block to the northwest and that of the Cathaysia Block to the southeast were conjoined by the Neoproterozoic collision that formed the SCC (Li et al., 2009; Wang P. et al., 2012). It is surrounded by the Philippine Plate and the paleo-Pacific subduction systems to the southeast and the India–China Block to the southwest. To the north, it is welded to the North China Craton by the Qinling–Dabie orogenic belt, and this amalgamation ended in the Late Jurassic (**Figure 1B**) (Zhang 1997; Faure et al., 2001; Faure et al., 2008). The subduction of the Pacific Plate began to play a significant role in the evolution of the SCC from the Mesozoic to Cenozoic (Chu et al., 2012b; Li et al., 2009; Zhang et al., 2019a, 2019b). The Early Mesozoic event in the central part of the SCC is referred to as the Indosinian Orogeny, and it was characterized by well-developed thrust faults, folds, and pervasive cleavage of the sedimentary cover as well as ductile syn-metamorphic deformation in the decollement layer and basement rocks. Some scholars have concluded that the NE–SW trending structures in the ESFTB are related to this Early Mesozoic event (Li et al., 2009; Shu et al., 2009).

2.2 Regional Geology of the Eastern Sichuan Fold-Thrust Belt

The ESFTB, located in the eastern margin of the Yangtze Block in the SCC, is recognized as a famous NNE–SSW-trending intracontinental orogeny and covers an area about 200 km wide and nearly 400 km long. The sedimentary strata are nearly continuous from the Precambrian to Cenozoic (with a total thickness of ~10 km), with several important unconformities (**Figure 3**). It is composed of two main lithological units: the Sinian to Middle Triassic marine sequence and the Upper Triassic to Late Jurassic–Early Cretaceous terrestrial sequence (Li, 2007; Li et al., 2015; Zhang et al., 2021a, 2021b, 2021c). The Neoproterozoic Banxi Group and its equivalents have generally been recognized as the folded basement of the Yangtze Block (Yan et al., 2003; Li et al., 2015). The Cambrian strata commonly consist of massive dolomite, gypsum, mudstone, and gray shale. The Ordovician strata consist of limestone interlayered with dolostone and argillaceous siltstone. The Silurian strata are composed of celadon shale and sandstone. The Carboniferous strata mainly consist of dolomite interlayered with clastic rocks and limestone. The Permian strata mainly consist of carbonate-rich rocks, whereas the Lower and Middle Triassic strata consist of limestone and dolomite layers interbedded with shale, mudstone, or sandstone. From the Upper Triassic to Cretaceous, the sedimentary series mainly occur in the Eastern Sichuan domain and are entirely continental facies sequences with red terrestrial clastic rocks (Yan et al., 2003; Wang et al., 2005; Shu et al., 2009). Based on the field exploration and seismic data, we found that most of the sedimentary stratigraphy was involved in the structural deformation system, which originated from the Lower–Middle Cambrian Longwangmiao–Gaotai regional detachment or the Lower Triassic Jialingjiang regional detachment within the core of the anticline (**Figure 4**).

From west to east, the structural style in the ESFTB varies from the Eastern Sichuan high-steep anticline belt to the Western Hunan–Hubei wide box-shaped anticline belt formed by the northeast-striking Qiyaoshan thrust fault. From north to south, in plane view, we discovered that there are distinct differences along strike based on a digital elevation map of the ESFTB (**Figure 2A**), and it can be divided into three sub-regions: 1) the northern E–W arcuate structural belt, 2) the middle NE–SW parallel structural belt, and 3) the southern N–S broom-shaped structural belt.

Due to the influence of the Dabashan Arc, the thrust structures in the northern E-W arcuate structural belt exhibit a tight arcuate geometry. The thrust belt is composed of a series of several subparallel ENE–WSW-striking anticlines. The Yunanchang, Longjuba, and Qiyaoshan anticlines and the northernmost part of the Fangdoushan anticline (**Figure 2A**) are characterized by intense folding and thrusting, and the arc-like structural belt buckles toward the NW direction in the plane. The middle NE-SW parallel structural belt is mainly composed of the Huayingshan, Tongluoshan, Mingyueshan, Jinghuashan, Fangdoushan, and Qiyaoshan anticlines (**Figure 2A**). The structure of the belt is characterized by high-steep dip angle anticlines; compared with the northern and the southern structural belts, the middle structural belt is more continuous and stable, with a parallel axis striking about N30°E. Based on the topographic profile A-A' (**Figure 2B**) and geological cross-section B-B' (**Figure 3B**), from west to east, the structural deformation system changes from trough-like folds and box folds to Jura-type folds. The southern N–S trending broom-shaped structural belt is composed of the Bayueshan, Yunwushan, Jinyunshan, Zhongliangshan, and Longwangdong anticlines from west to east (**Figure 2A**). These anticlines are branch structures of the Huayingshan anticline, and the orientations of their axes are not parallel and change from N30°E to N40°E in the west to S–N in the east.

3 EXPERIMENTAL PROCEDURE AND ANALYTICAL TECHNIQUES

The physical tectonics simulation experiments were mainly conducted to study the geological structural deformation; using the experimental model simulation method, the formation process of the orthogonal tectonic phenomena in the field was investigated, and the morphological characteristics during each stage of the deformation process

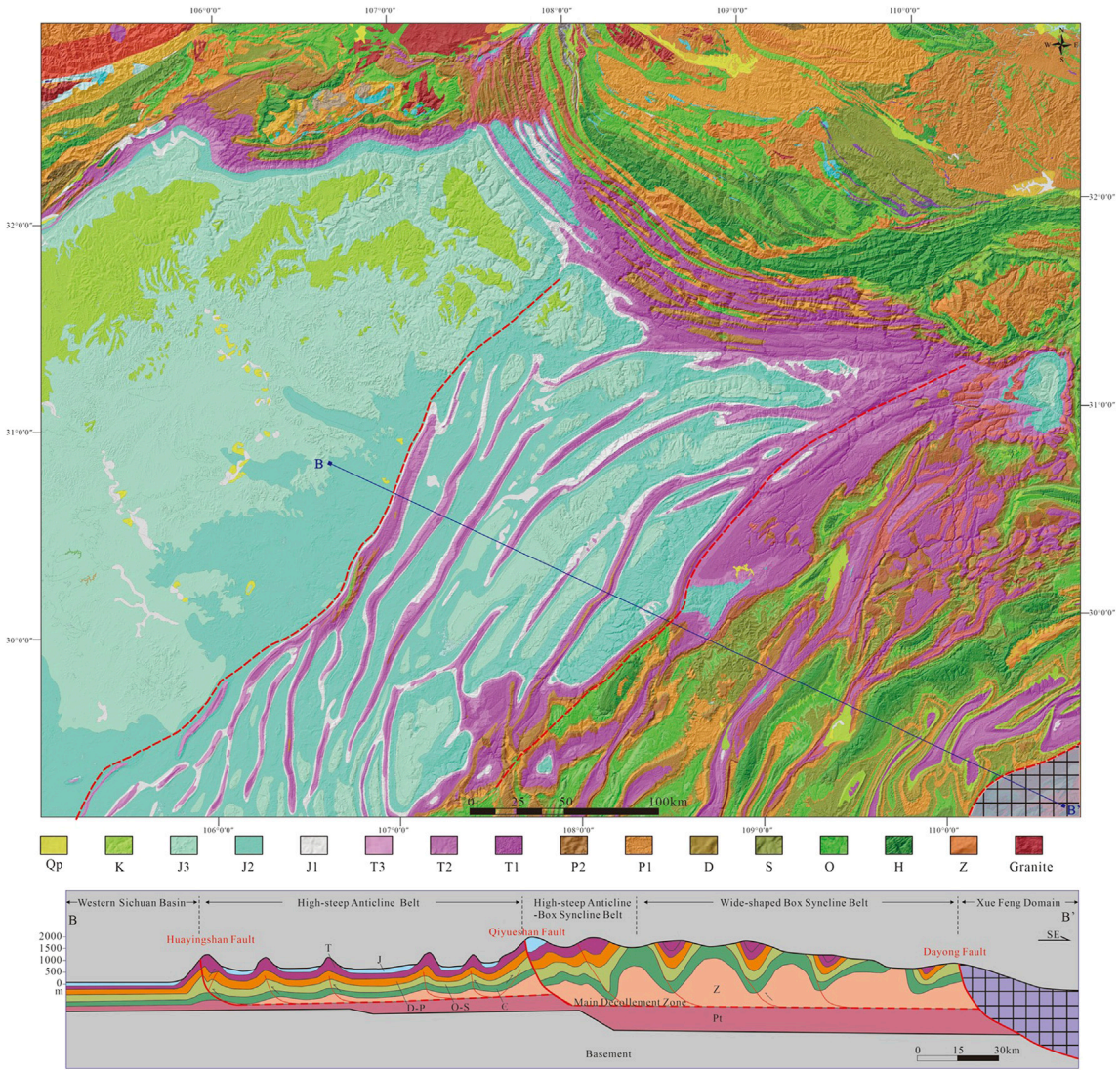

FIGURE 3 | Simplified geological sketch map and cross section of the Eastern Sichuan basin.

were observed. This is one of the most effective methods of studying the forced deformation of laminated materials (Buchanan and Mc Clay 1991; Zhou et al., 2007; Yan et al., 2016).

3.1 Modeling Strategy

The experimental setup used for the physical simulation experiments in this article was obtained from the tectonophysical simulation laboratory of the Key Laboratory of Tectonogenesis and Metallogenesis, Ministry of Land and Resources, Chengdu University of Technology (**Figure 5A**). The size of the experimental sandbox was 100 cm × 60 cm × 40 cm, and the experimental device used a hydraulic system to provide the required stress. The system can be used to conduct simulation experiments involving extrusion, tension, augmentation, bottom incision, shearing, and bottom shearing. The steps of the experimental process, according to the experimental model, included laying the experimental materials, opening the experimental control system, setting the speed and running distance of the pusher, and running the pusher to conduct the experiment. During the experiment, a digital camera was used to monitor the side and upper surfaces of the experimental model in real time and to collect the experimental data.

As was discussed by Hubbert (1937), our methodology is based on the geometry, material, dynamic, time, and boundary similarity principles, which focus on the validity of the tectonic analog experiments. Simulation experiments conducted on this basis can reflect natural processes more scientifically (Bonini et al., 2012; Yan et al., 2016).

3.2 Material Properties and Model Scaling

To produce a fold-thrust belt in our physical models, appropriate analog materials were used to simulate the upper crust. These materials were characterized by their elastic-frictional plastic behavior. We employed quartz sand, which is a granular

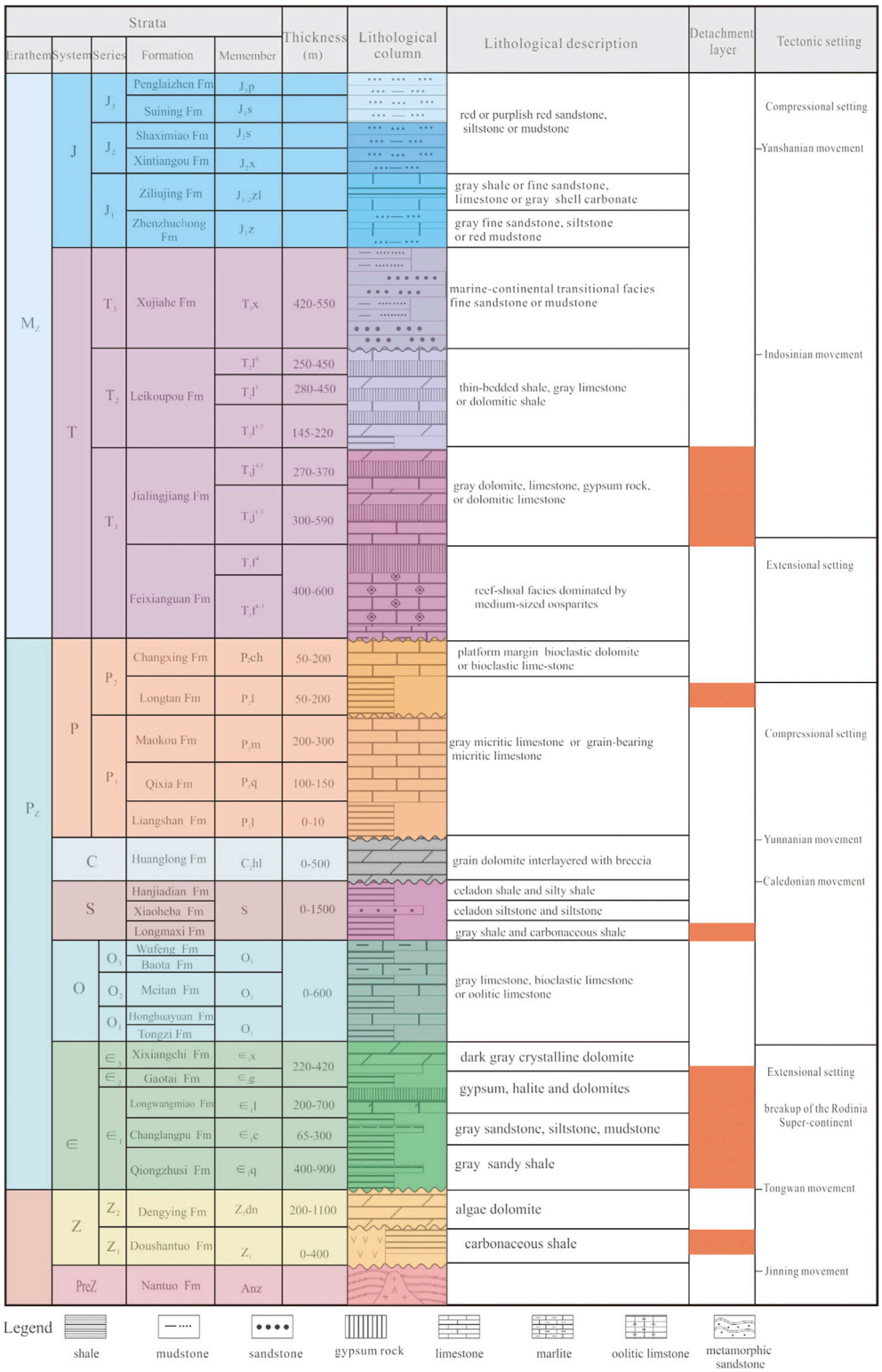

FIGURE 4 | Stratigraphic column of the Eastern Sichuan fold-thrust belt with the location of potential décollement zones (modified after Li 2015).

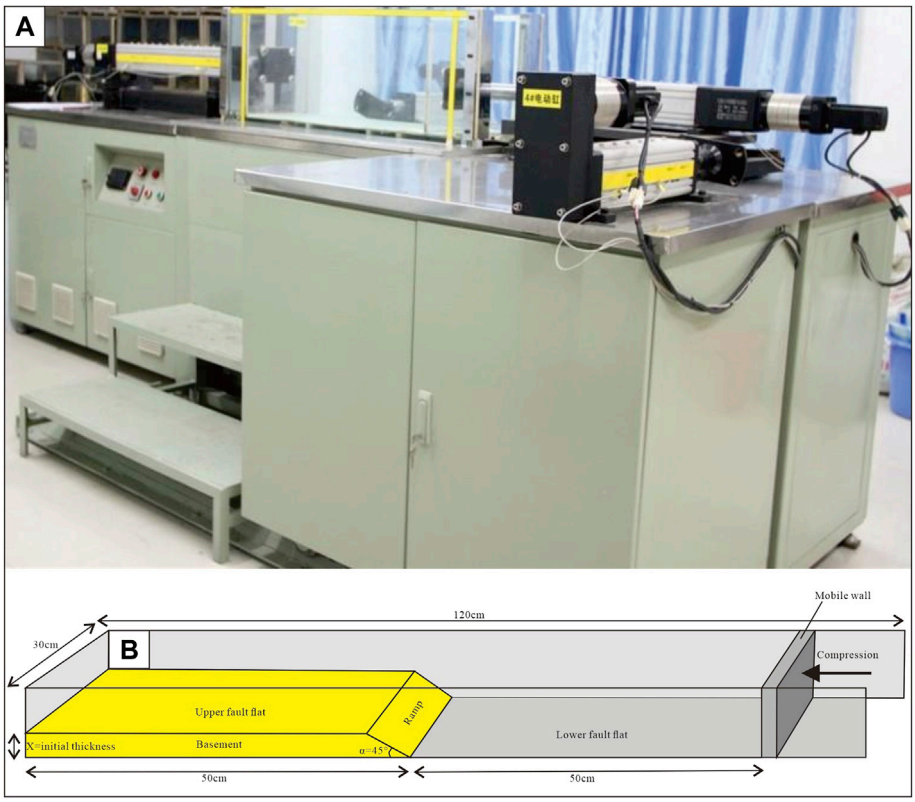

FIGURE 5 | (A) Key Laboratory of Tectonics, College of Earth Sciences, Chengdu University of Technology. **(B)** Experimental apparatus with model dimensions and details of all experiments.

material used in nearly every simulation of brittle deformation due to its potential to generate kink folds (Mulugeta and Koyi 1992). Because of its low cohesive force, quartz sand is ideal for simulating brittle deformation of the upper crust. Furthermore, we used glass microbeads, which have a lower cohesion strength than quartz sand and are therefore weaker (Panien et al., 2006) The diameter of the microglass beads used was about 0.3 mm, and the internal friction angle was about 25° (Mulugeta and Koyi, 2006). Researchers have suggested that these beads can be used to simulate relatively weak competent rocks such as carbonates, mudstone, and shale. A silica gel is an ideal material for simulating the slippage layer in the cap layer in physical simulation experiments. Silicone with a viscosity of less than 5×10^4 Pa-s has Newtonian fluid properties at low strain rates (Graveleau and Dominguez, 2008). In the experimental model, a silica gel was mainly used to simulate the paste saltstone slip layer in the septal-folded cover. Green quartz sand was used as a marker layer in the experiment, and its physical properties were the same as those of the undyed quartz sand.

The boundary conditions of the formation, thickness of the brittle/ductile layer, extrusion velocity, differential stress, basal shear stress, ductile layer shear stress, brittle/ductile ratio, shear strain rate, and geometric features of the brittle and ductile layers were focused on according to the physical simulation similarity principle (**Table 1**) in order to meet the requirements of the experimental study (Hubbert 1937). The experimental model was initially 100 cm long, 60 cm wide, and 30 cm high. A large amount of low-temperature thermochronological data indicate that the main formation age of the Eastern Sichuan fold belt is 165–75 Ma (Mei et al., 2010; Li et al., 2011; Wang W. et al., 2012). Based on equilibrium section data, previous scholars have determined that the Eastern Sichuan fold belt was shortened by a total of about 140 km during the Late Jurassic–Late Cretaceous, with a total shortening of about 32%, including 72.5 km on the southeast side of the Qiyue Mountains and 67.5 km on the northwest side of the Qiyue Mountains (Mei et al., 2010; Wu et al., 2019). Therefore, in the model, the squeezing pressure was applied from the right side to push the right active end toward the left, and the total shortening was 320 mm, with the same shortening rate of 32%. In order to reveal the maximum possibility and the most complex deformation characteristics of the sandbox model and the geological processes in the most effective timeframe, the choice of a low speed and reasonable effective extrusion speed was crucial for the mechanism of the sandbox model simulation (Zhao 2017). In the simulation test, the speed of the pushing plate was set to 0.01 mm/s so that we could successively observe a clear and comprehensive deformation process of the sandbox wedge and the construction style. In the experiment, the kinetic similarity between the physical model and the prototype is as follows:

TABLE 1 | Scaling parameters between models and nature.

Parameter	Model	Nature	Model/nature ratio (*)
Particle size (mm)			
-Dry quartz sands	0.2	-	-
-Glass microbeads	0.3	-	-
Ductile-layer viscosity	8.3 × 103 Pa s	1 × 1,018 Pa s	η^*≈8.3 × 10–15
Internal friction	0.65	0.60–0.85	u^* = 0.76~1.08
Density (g/cm3)			
-Dry quartz sands	1.3[a]	-Brittle layer 2.4–2.8[b]	ρ^* ≈0.5
-Glass microbeads	1.4[c]	-Ductile layer 2.4–2.8[b]	ρ^* ≈0.5
-Silicon putty	0.83	-Detachment layer 2.2	ρ^* = 0.38
Gravity acceleration	9.8 m/s^2	9.8 m/s^2	g^* = 1
Length, l	1 m	200 km	L^* = 5 × 10–6
Stress, σ			
-Dry quartz sands	100–150pa[b,d]	40–60 MPa 12 MPa	σ^* = ρ^*×g^*×L^* = 2.5*10–6
-Glass microbeads	30pa[b,e]	-	-

[a]*Wang et al. (2016)*
[b]*Gomes (2013)*
[c]*Panien et al. (2006)*
[d]*Eisenstadt and Sims (2005)*
[e]*Krantz (1991)*

$$\sigma^* = \rho^* \times g^* \times L^*, \quad (1)$$

where σ* is the stress ratio between the model and the prototype; ρ^* is the density ratio; and g* and L* are the gravitational acceleration and length ratios, respectively. The experiments were conducted in a normal gravity field; so, the ratio of the gravitational acceleration was $g^* = 1$. The density ratio was $\rho^* \approx 0.5$, i.e., the density of the experimental material was approximately equal to half the density of the stratum.

In the experiment, the 1000-mm model represented about 200 km of the geology in Eastern Sichuan; so, the similarity coefficient was about

$L^* = 5 \times 10^{-6}$ and 1 cm = 2 km in the model.

The viscosity of the stratum was about 1×10^{18} Pa·s. The viscosity of the silicone was 8.3×10^3 Pa·s. The viscosity similarity factor was $\eta^* \approx 8.3 \times 10^{-15}$.

$$\eta^* = \sigma^* \times t^*. \quad (2)$$

Based on **Eqs 1**, **2**, $t^* \approx 3.3 \times 10^{-9}$, i.e., 1 h of simulated time was equal to 3.5×10^4 a of geological time.

3.3 Experimental Setup and Method

It is better to design multiple groups of comparison tests for the experimental design because through comparison of multiple groups of experiments, the influence of each variable in the model on the experiment can be analyzed and the influences of the experiment-related elements on the experiment can be clarified. According to the specific geological formations in the study area, the model size and the running rate of the pusher were calculated according to the similarity ratio principle, and the experimental model was finally designed. We conducted six experiments in a 100 cm (length) × 30 cm (width) × 30 cm (height) deformation box (**Figure 5B**). The box was composed of a flat, horizontal base plate bounded by two fixed lateral glass walls and two vertical plastic walls, one of which was mobile (the backstop) and the other was fixed. The model deformation was accomplished by moving the mobile wall using a screw-jack controlled by a stepper motor. All of the model devices are shown in **Figure 6**. In sandbox analog models, the friction along the glass walls is not negligible, but the impact of the lateral friction is even greater in models with basal friction (Vendeville 2007; Soulouniac et al., 2012). However, these negative factors can be totally avoided if a thin silicone coating is applied to the lateral walls (Costa and Vendeville, 2002; 2004; Koyi and Cotton, 2004). We reduced the influence of the lateral friction between the sand and the glass sidewalls by lubricating the glass walls with a viscous coating, thus minimizing the lateral friction that could affect the kinematics during the experiments.

The tectonic shortening rate in the Eastern Sichuan area in the Mesozoic (165–75 Ma) was about 32%. The Qiyue Mountain Fault was an important pivot for the transition from septal to septal folding and was a product of the northwest migration of the shallow part of a pre-existing high-angle fracture. The dip angle of the Huaying Mountains Rift controlled the wavelength of the septal folds, and a steeper dip angle (45°) was more favorable for the development of typical septal folds (Wu et al., 2019).

The sandbox simulation experiments were divided into six groups (**Figure 6**), and the specifications of the layout of the materials in the model were 1000 × 300 × 30 mm (length × width × height). In experiment 1, only quartz sand was used as the experimental material to simulate rigid ground. There was a 10-mm basement step at the fixed end above the extrusion end, and the step surface had a dip angle of 45°. Half of the 250–750-mm high and low step surfaces were laid at each side. In experiment 2, as a comparison experiment to experiment 1, the other conditions were the same, but the quartz sand was replaced by microglass beads (**Figure 6B**). In experiment 3, the

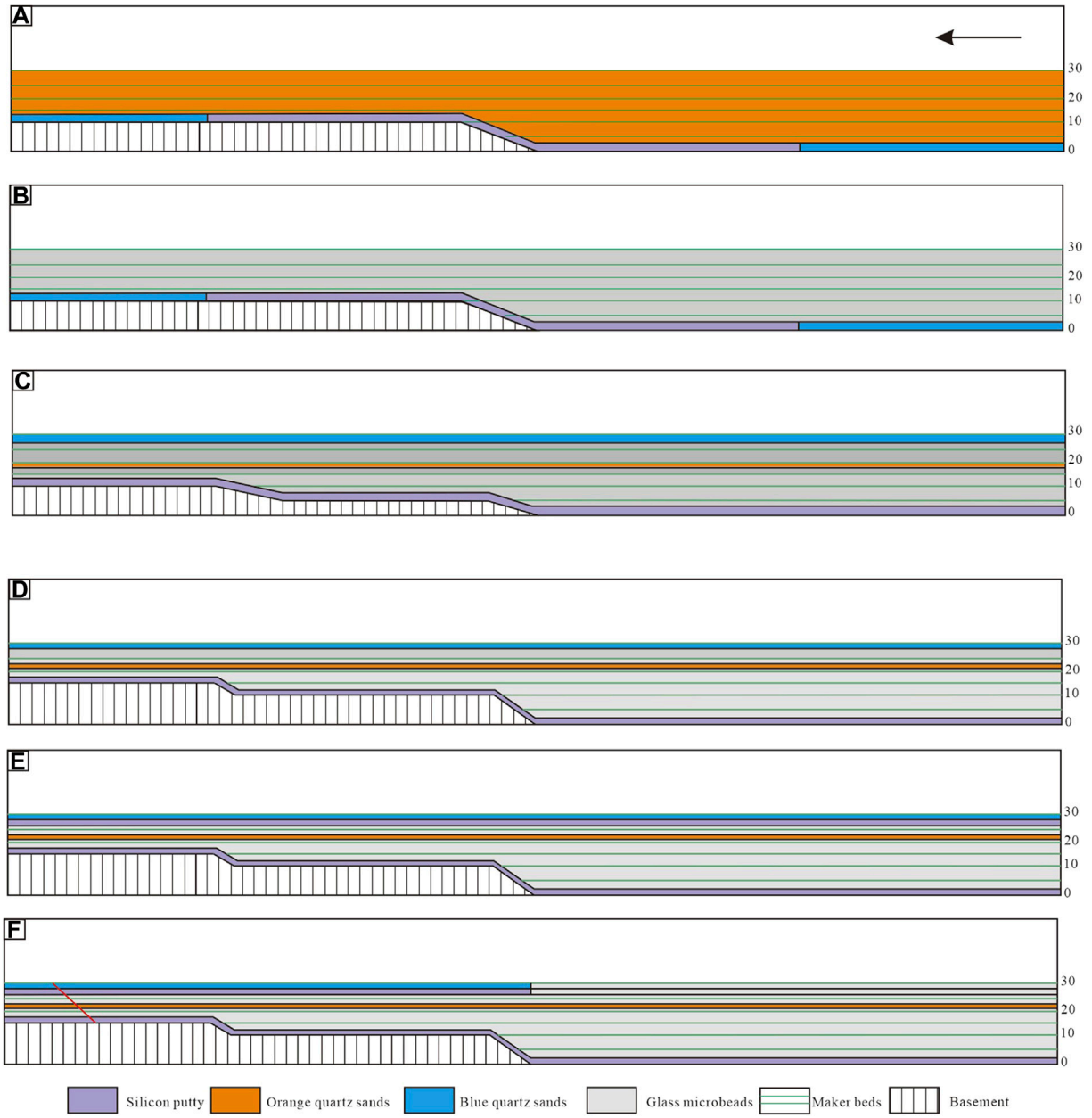

FIGURE 6 | Sketch showing the model configurations.

substrate step was set to a two-step substrate rising state. One step of 500 mm at the substrate, followed by another 750-mm step, constituting a step above the level of 5 and 10 mm rigid substrate (**Figure 6C**). The micro-glass beads were used to form the basal layer, and 2.5-mm quartz sand was used to form the middle and top layers to simulate a rigid ground sandwich and a cover layer, respectively. In addition, 3 mm of silicone was uniformly spread across the bottom of the model. In experiment 4, as a comparison experiment to experiment 3, the materials used were the same, but the heights of the two steps were changed. The steps for experiment 5 were the same as those for experiment 4, but a 2-mm-thick layer of silicone resin was added to simulate double-layer slip tectonic deformation (**Figure 6E**). Experiment 6 was based on experiment 5, but only the second layer of silicone resin was laid on the elevated part of the basement, and the silicone resin and quartz sand cover were replaced by microglass beads in the unelevated area of the basement, which is consistent with the regional geological map. This is in general agreement with the fact that the Triassic and Jurassic strata in the intertrench area have been almost stripped away, and a metal baffle with an inclination of about 45° was added at

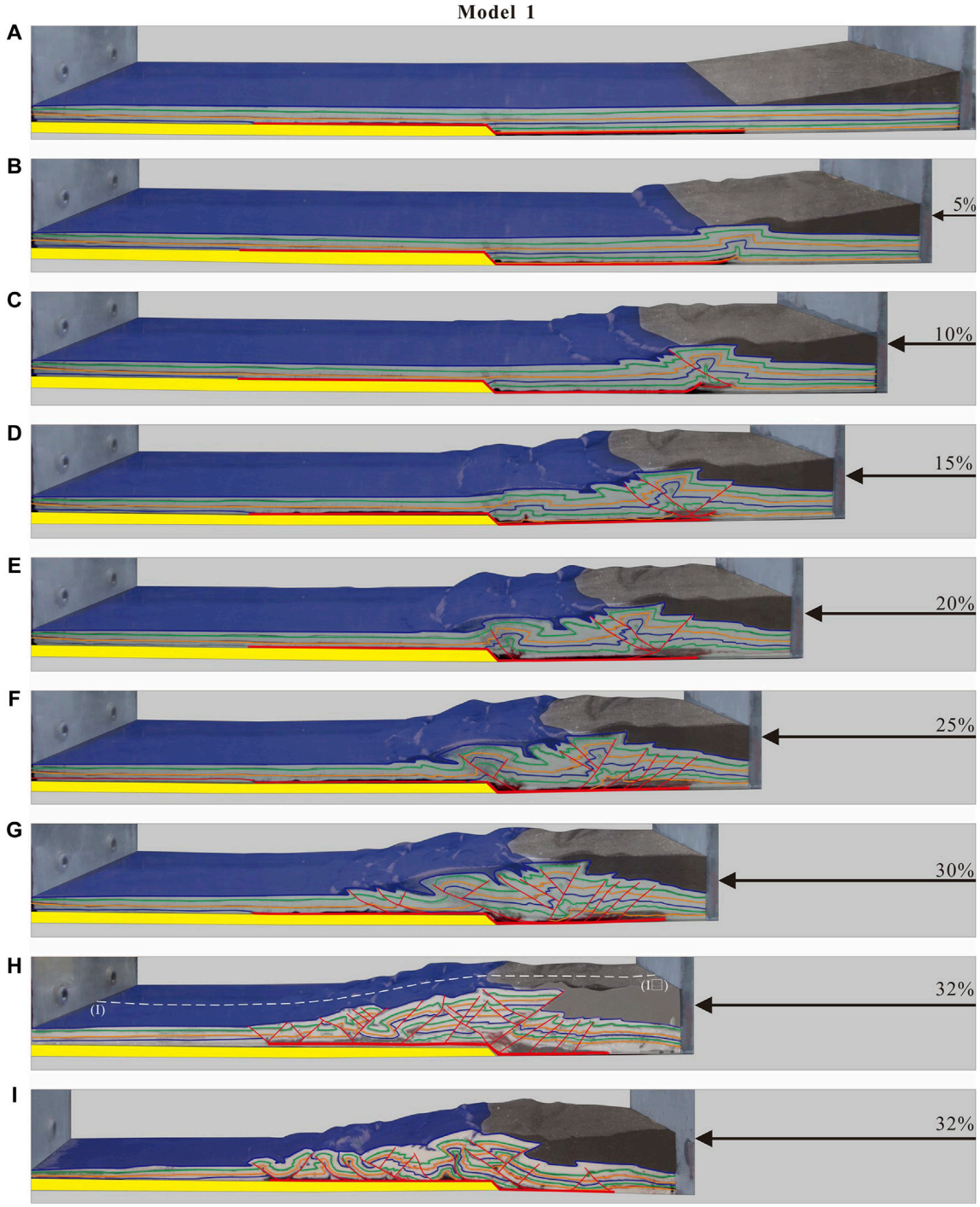

FIGURE 7 | Sequential deformation features of model-1.

the fixed end of the model to simulate the pre-existing polished fracture (**Figure 6F**).

3.4 Experimental Limitations

The complexity of natural tectonic deformation, such as multi-phase superimposed deformation, syn-tectonic deposition, and the influence of denudation on staged-growth deformation, was not considered; so, the model did not fully compensate for the control of the deformation due to denudation. The model starts with the main controlling factors and simplifies the influence of the microscopic heterogeneity according to the composition of the stratigraphic rocks. This is

an idealization and simplification of the geological prototype, especially because there are multiple sets of slip layers in the area, while the model uses a maximum of two slip layers. It should be noted that deep geophysical data such as the seismic reflection profile and magnetotelluric profile were analyzed (Zou 2011; Deng et al., 2014). There are some limitations in the distribution of the gypsum layer in Eastern Sichuan, and the heterogeneity of the slippage layer could not be fully reflected in the experiments. Thus, the control of the influence of the slip layers on the cover in the experimental model was not ideal, and it is necessary to further explore the influence of complex factors, such as multi-layer slip layers plus the basement morphology, on the folded and alluvial zones in East Sichuan.

4 RESULTS

4.1 Group 1

Figure 8 illustrates the seven deformation stages in experiment 1. In the shortening stage of the extrusion, a low amplitude slip knee fold was formed at the junction of the silicone-layered bottom plate and the non-silicone-layered bottom plate, and this knee fold further developed into a box fold (**Figure 7A**). As the compression rate increased, a tile-like recoil wedge formed in front of the movable baffle, and the undeformed sand body kept proliferating into the wedge to form a new recoil fault. The size of the wedge increased continuously. When the compression rate was 15%, the first recoil fault was formed, which only absorbed a very small part of the displacement, after which it soon ceased to be active. At a shortening rate of 20–32%, the previously formed fault rotated, and the fault yield changed as the deformation was continuously transmitted. The recoil fault yield became more gentle, and conversely, the recoil fault yield became steeper, leading to gravitational slip collapse, causing the upper plate of the fault to slide downward along the fault surface, thus causing the fault slip distance to gradually decrease as well.

From the cross-section (**Figure 7I**), it can be seen that the new rebound faults were developed under the old ones, and they extended in a sequential manner toward the foreland, i.e., in a foreshortened manner. Then, the other tectonic units were formed one by one in the foreland in the same way (**Figures 7E–H**), and some small recoil faults began to develop in the upper and middle tectonic layers, slightly deforming the strata.

4.2 Group 2

In experiment 2, the quartz sand in experiment 1 was replaced with microglass beads, and at first, the initial horizontal stratum began to slide and form the first fold (d = 5%) along the silica-lined and nonsilica-lined locations under the compression applied by the right movable baffle (**Figure 8B**). At d = 10%, small fault propagation folds began to develop and the model became active at the basement uplift site and was the first to form a second fold (**Figure 8C**). As the extrusion continued, the fault propagation folds led to the uplift of the overlying strata. The front flank of the fold became steeper, while the back flank became shallower, and inverted folds (d = 15–20%) were gradually formed (**Figures 8C, D**). At this point, the basement tectonic layer had a tendency to thicken, but the overall deformation was not obvious, and the model deformation in this stage did not occur sequentially from right to left. Then, slight uplift (d = 25%) occurred and shifted successively forward on the elevated basement surface (**Figure 8F**). When the shortening rate was d = 30–32%, the slip effect propagated farther, and three more tightly closed back-slope folds and three wide slow oblique style folds were formed in turn at intervals (**Figures 8G, H**). At this time, the model results were closer to the slot-blocking transition zone tectonic morphology. At this point, the model results were closer to the tectonic pattern of a channel-blocking transition zone.

4.3 Group 3

Figure 9 shows the overall simulation process of experiment 3. In this experiment, in order to explore the influence of the basement uplift height and the combined morphology of energetic and non-energetic strata on the experimental simulation results, the basement steps were set at two step-like basement uplifts; and silicone, microglass beads, and quartz sand were used to represent the actual stratigraphic slippage (e.g., paste salt rock and shale), non-ergodic layers (e.g., thin-slabbed tuff and dolomite), and andergodic layers (e.g., thick layers, massive tuff, and sandstone) in the East Sichuan area, respectively. The stages of the entire evolutionary process are explained later in detail.

At d = 5%, the basal tectonic layer started to shorten locally under the compression applied by the right movable baffle, leading to folded uplift of the overlying strata (**Figure 9B**). Unlike in experiment 2, the central tectonic layer and the upper tectonic layer in experiment 3 did not change uniformly, with thickening or thinning anomalies between the layers, forming a fold deformation pattern with thick top and thin flanks. When d = 10–15%, the basement tectonic layer gradually developed basement retrograde faults (three at this time) (**Figures 9C, D**). These basement retrograde faults together formed the double basement structure, which led to the thickening of the strata in the vertical direction. However, the actual increase in the stratigraphic thickness was not significant because the angle of the retrograde faults at this point was not high and the break distance was small. As the baffle continued to move to the left, at a shortening of d = 20%, plastic flow occurred on the first elevated step, i.e., there was local deformation at the leading edge, resulting in a small amount of uplift of the overlying strata (**Figure 9E**). The occurrence of deformation indicates that the stress was no longer confined to the double structure at this point, and it begins to be transmitted forward. When d = 25–32% (**Figures 9F–H**), the number of basement retrograde faults on the first-stage bench increased again, and all of the faults broke through the upper tectonic layer, allowing more fold patterns to develop on the leading edge of the retrograde region. The final section morphology of this experiment is shown in **Figure 9I**. The second-stage terrace experienced

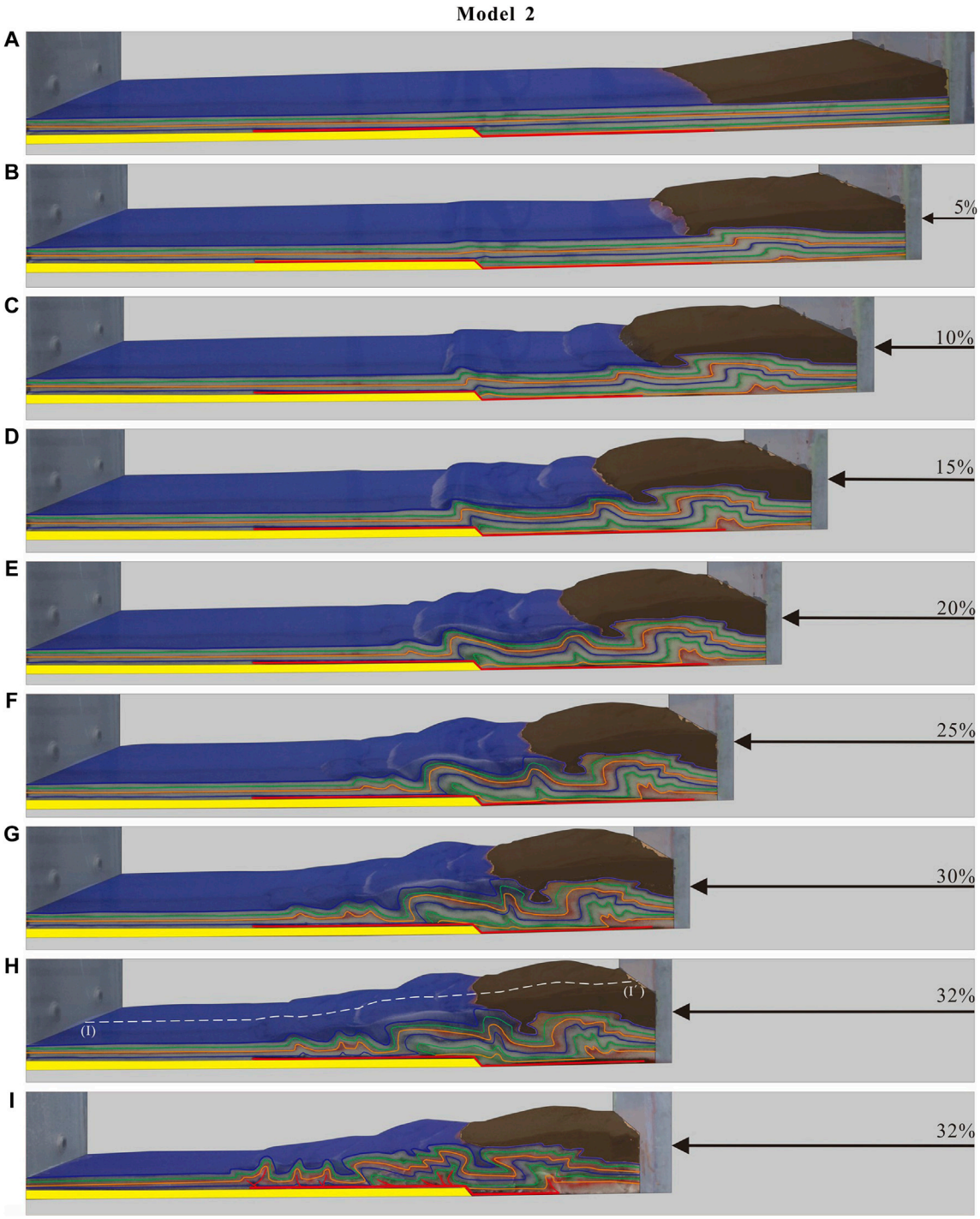

FIGURE 8 | Sequential deformation features of model-2.

almost no transfer deformation, and a box-like backslope with an oblique style with wavelengths of nearly 1:1 in the frontal zone of the first-stage terrace was formed, with steeper production on both flanks and flatter and wider turning ends. This is different from the high steep and tightly closed backslope morphology in the Eastern Sichuan area.

4.4 Group 4

Considering that the final deformation of experiment 3 did not propagate above the second step surface even when its shortening rate reached the maximum, in order to discuss the effect of increasing the height of the basal uplift and thinning the thickness of the cover on the propagation distance, in experiment 4, the

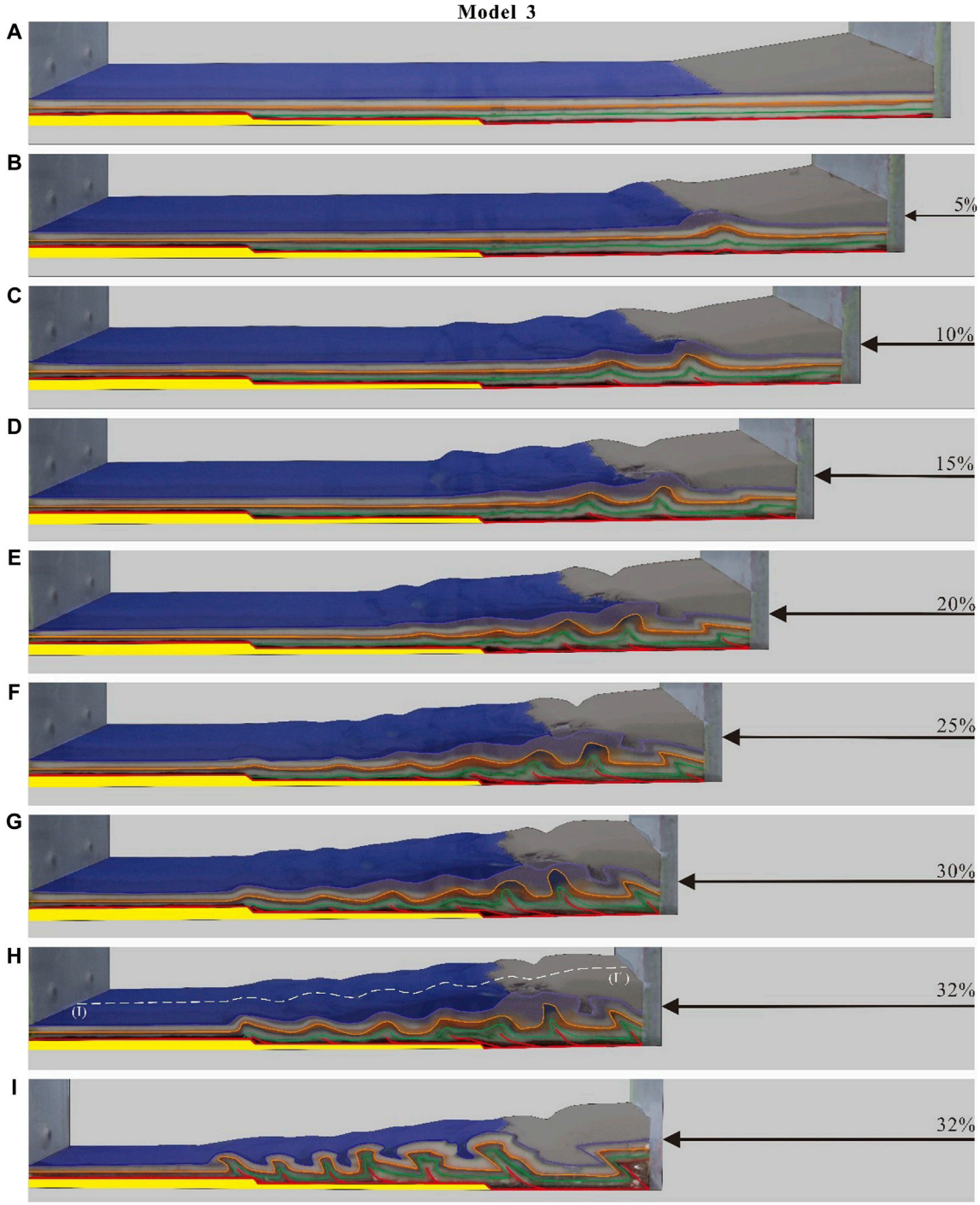

FIGURE 9 | Sequential deformation features of model-3.

heights of the two steps were increased by 5 mm based on the setup of experiment 3 (**Figure 7D**).

When the shortening rate was d = 5%, a box-like slip fold first developed near the extrusion end (**Figure 10B**); and at the same time, a slight bulge developed in the first step elevation area due to the blocking effect of the rigid base plate. As the extrusion proceeded, when d = 10%, a foreshortening fault developed on each of the two front flanks of the first two box folds, and the faulting also made the original single-fold pattern more complex (**Figure 10C**). When d = 15%, a third fold formed between the first two, and the backslope pattern was steep on the front flanks and shallow on the back

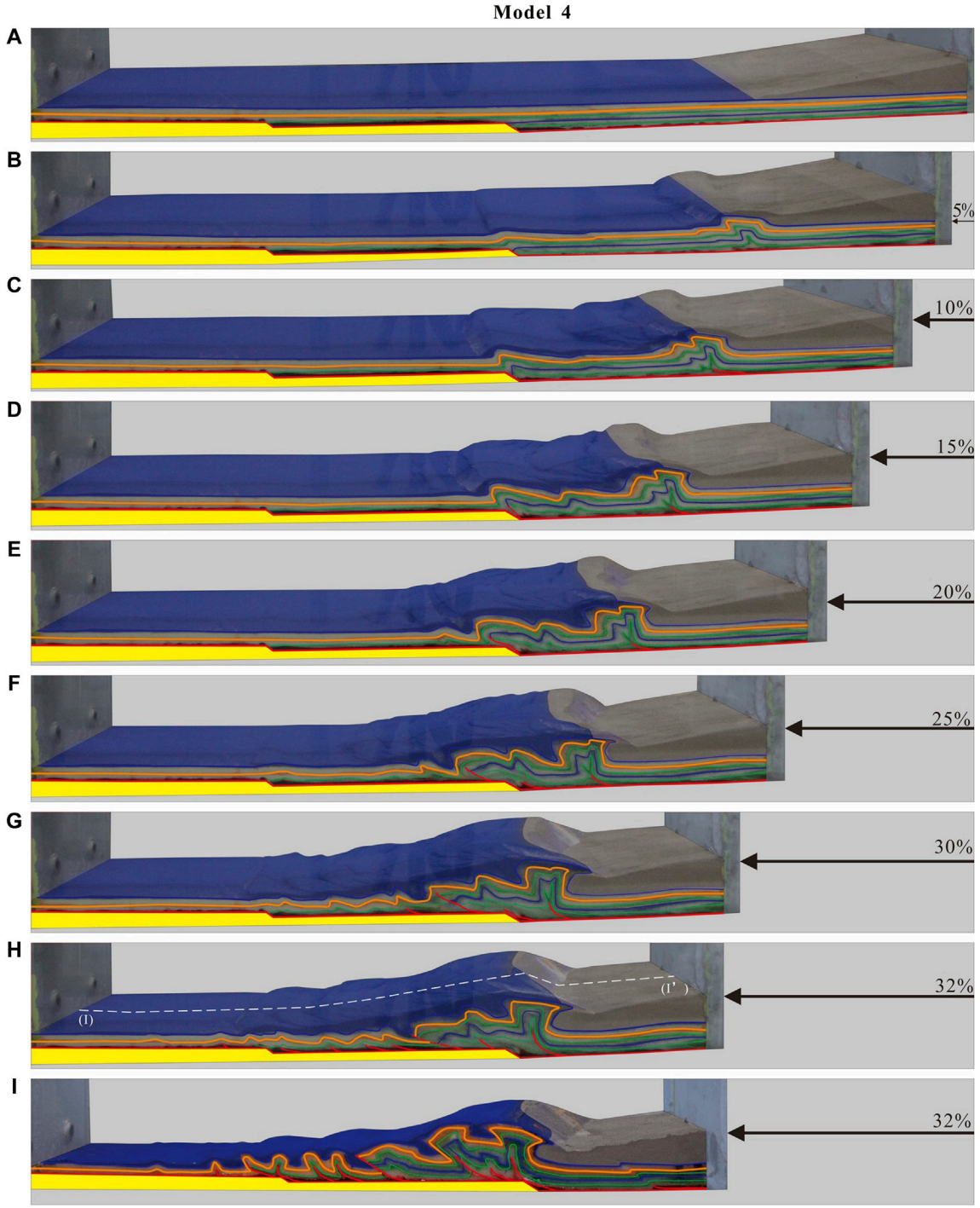

FIGURE 10 | Sequential deformation features of model-4.

flanks at this time (**Figure 10D**). As the shortening rate increased (d = 20–25%), the fold wavelengths in the trailing edge tectonic zone were compressed and shortened. At this time, the oblique was tightly closed, while the dorsal slope was wide and shallow, and the model exhibited a septal groove fold style (**Figure 10F**). It can be clearly seen from the cross section that when d = 32% (**Figure 10I**), the tectonic units were produced successively on the three platforms (high, middle, and low) formed by the two-step height change sites. Both experiment 4 and experiment 3 had the same total shortening rate, but model 4 developed significantly more tectonic units than model 3; so, the elevation of the base ahead

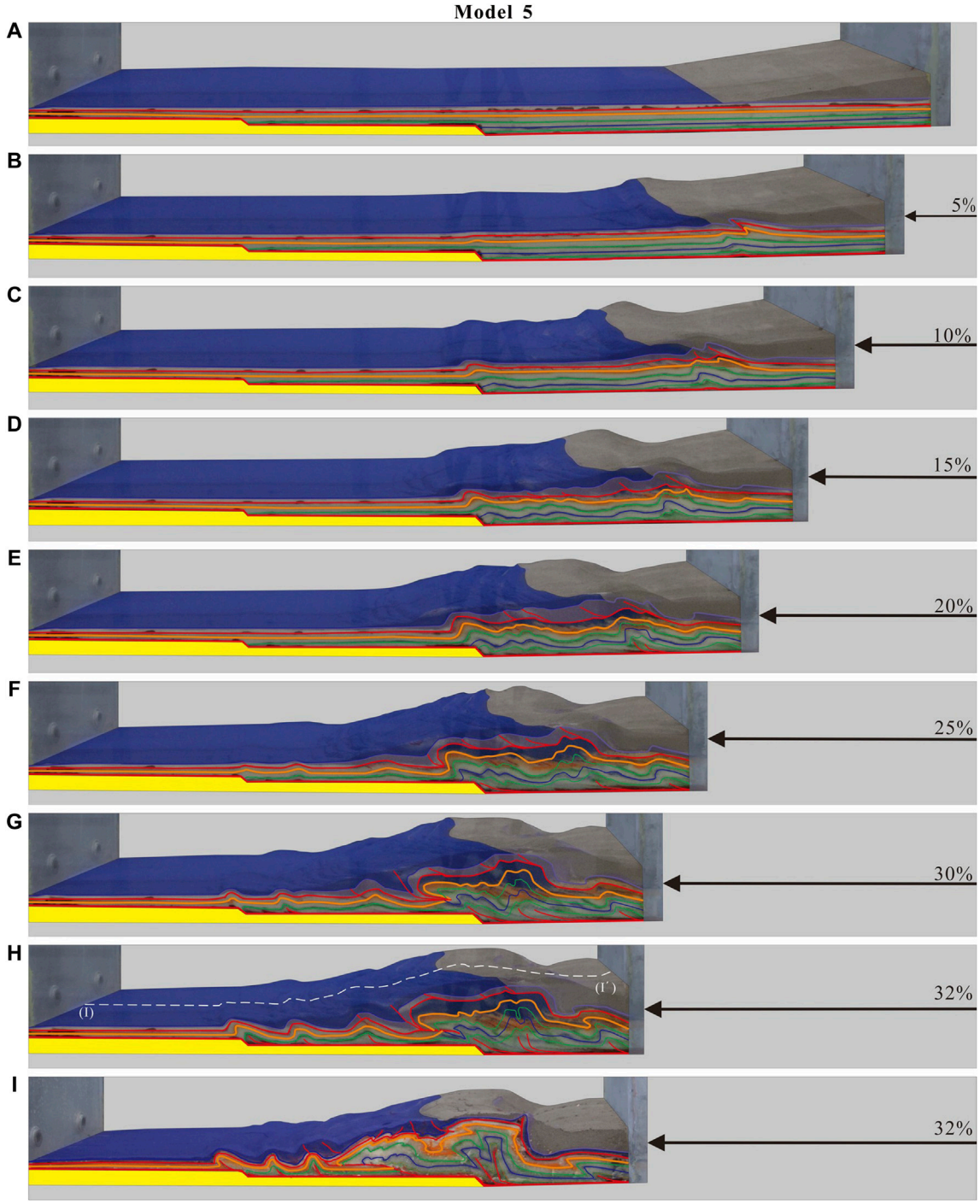

FIGURE 11 | Sequential deformation features of model-5.

of the extrusion and the thinning of the cover thickness obviously caused the slip action to propagate further. The folds developed on the highest terrace were characterized by narrow dorsal and wide diagonal folds, and the model's tectonic frontal zone contained the beginning of a Jurassic-style fold pattern.

4.5 Group 5

In experiment 5, we set up two sets of slip layers in the model to study the overall kinematic evolution of the fold punch-off system, and the bottom layer of silicone was used to simulate the gypsum and shale of the Lower–Middle Cambrian Longwangmiao Formation and Gaotai Formation. The upper

silicone layer was used to simulate the dark gray gypsum-bearing dolomite of the Lower Triassic Jialingjiang Formation.

Figure 11 shows the deformation process of model 5 with increasing shortening. When the compression was d = 5%, model 5 was also the first model in which the upper tectonic layer was the first to appear in the antecedent direction of the retrograde fault. The bottom of the upper plate of the fault thickened, the thickness of the top layer remained basically unchanged, the level bent, and a fault propagation fold was formed. The deformation was weaker in the lower tectonic layer than in the upper tectonic layer. Subsequently, the second and third faults, which rushed to the foreland in the direction of the first fault, formed in succession, and their development process was similar. The upper plate of the fault formed fault propagation folds (d = 10–15%). As the shortening increased, the thickness of the upper layer basically remained unchanged, the fault no longer developed, and the level continued to bend under the influence of the change in the fault production. The lower tectonic layer deformed relatively strongly, forming fault propagation folds, and the fold pattern was mainly compound (d = 20–25%). Under continued compression to 32%, i.e., to the final form of the model, due to the action of the double-layered slip layer, the model underwent layered deformation. Finally, the model's morphology became very complex near the root zone near the extrusion end, while the frontal zone transitioned from the compartmentalized groove zone fold style to the compartmentalized fold style. It should be noted that the propagation distance of model 5 was shorter than that of model 4, and the deformation propagation did not reach the highest step surface. This may have been caused by the formation of more foreshortening fault displacement in the upper slip-off tectonic layer during the extrusion process, which absorbed a considerable proportion of the energy.

4.6 Group 6

Based on the information gained from the results of experiment 5, we simulated the actual geological conditions of the ESFTB. We made the following changes to the setup of experiment 6: first, we kept the double-layer slip system composed of the upper and lower silica resin layers at the fixed end, and since the tectonic layers above the Jialingjiang Formation in the western part of Xiangjiang have basically experienced denudation, the upper slip layer on the mobile side was eliminated, and all of the silica resin and quartz sand on this side of the model were replaced with microglass beads. Second, considering that the low-temperature thermochronological data show that the polished backslip formed earlier than the adjacent backslip to the east (Richardson et al., 2008; Wang P. et al., 2012), a metal sheet with an inclination of 45° was added to the highest step plane at the fixed end of the model to simulate the pre-existing polished fracture (**Figure 7F**).

The seven stages of the deformation of model 6 are shown in **Figure 12**. When d = 5%, the extrusion end and the first basement height uplift site were the locations of the stress concentration, and two boxed backslopes were formed first, with the axial surface tending to slope toward the extrusion end (**Figure 12B**). When d = 10%, the sequence of formation of the tectonic units did not develop one by one toward the front edge, and the stratum began to uplift between the two backslopes. When d = 15% compression, two vectors and three backslopes were formed at the back edge (**Figure 12C**). As the compression continued to increase (d = 20–25%), the backslope became wider and shallower, while the diagonal became increasingly more tightly closed, forming a typical septal fold (**Figure 12D**). During this stage, fault slip folds started to form on the first uplift plane and at the second uplift site. It can be seen from the model that the main slip layer controlling the deformation at this time was the lower slip layer (**Figure 12E**). In contrast to the previous experimental model, when d = 25–30%, the deformation of the physical model propagated quickly to the left, and folds began to rumble both on the third step plane and at the location where the metal sheet was buried, forming three tightly closed backslopes. The model cross section at d = 32% shows that the overall tectonic style of the section was dominated by the development of an extrusion-formed stacked tile structure (**Figure 12I**), and the main tectonic deformation occurred between the upper and lower silicone layers, with strong stratigraphic deformation between the silicone layers and the development of multiple backlash fractures and fault-related folds. The model's trailing edge zone exhibited a typical septal groove style of folding, and the leading edge zone exhibited a typical septal block style of folding.

5 DISCUSSION

5.1 Controls on Modeled Structural Styles

Model 1 was capped by quartz sand, and the capping deformation was dominated by faults. However, folds were difficult to form, and even when they were formed, they were quickly destroyed via fault modification. In model 2, the quartz sand was replaced with microglass beads. The structural style formed was dominated by folds, and the fracture did not damage the fold flanks to a large extent. Therefore, the folding-impulse fault zone deformation style was influenced by the brittle shear strength and basal ductile shear strength to a certain extent. Moreover, the lithology of the cover layer in the folding area should not be that hard or soft in the deformation stage; otherwise, a series of foreshortening stacked tile-like recoil pushover structures and recoil fault structures will form.

Model 2 deformed significantly in the layer above the silicone layer, while the non-silicone layer was not deformed or was insignificantly deformed, indicating that the silicone slip layer effectively reduced the friction at the bottom of the model. In addition, the slip layer was necessary for the formation of slip faults and fault-related folds, and it controlled the overall evolutionary process of the ESFTB. From the deformation propagation process, the lower burial depth of the slip layer and the thicker cover layer in models 1–3 compared to models 4–6 limited the effective propagation distance. The formation sequence of the tectonic units did not develop from the extrusion end to the leading edge one by one. The units developed earlier at the basement uplift site or near the basement friction change zone, and the tectonic units at these locations entered the active state earlier, thus increasing the transmission distance of the slip layer in the leading edge direction. It should be noted that the

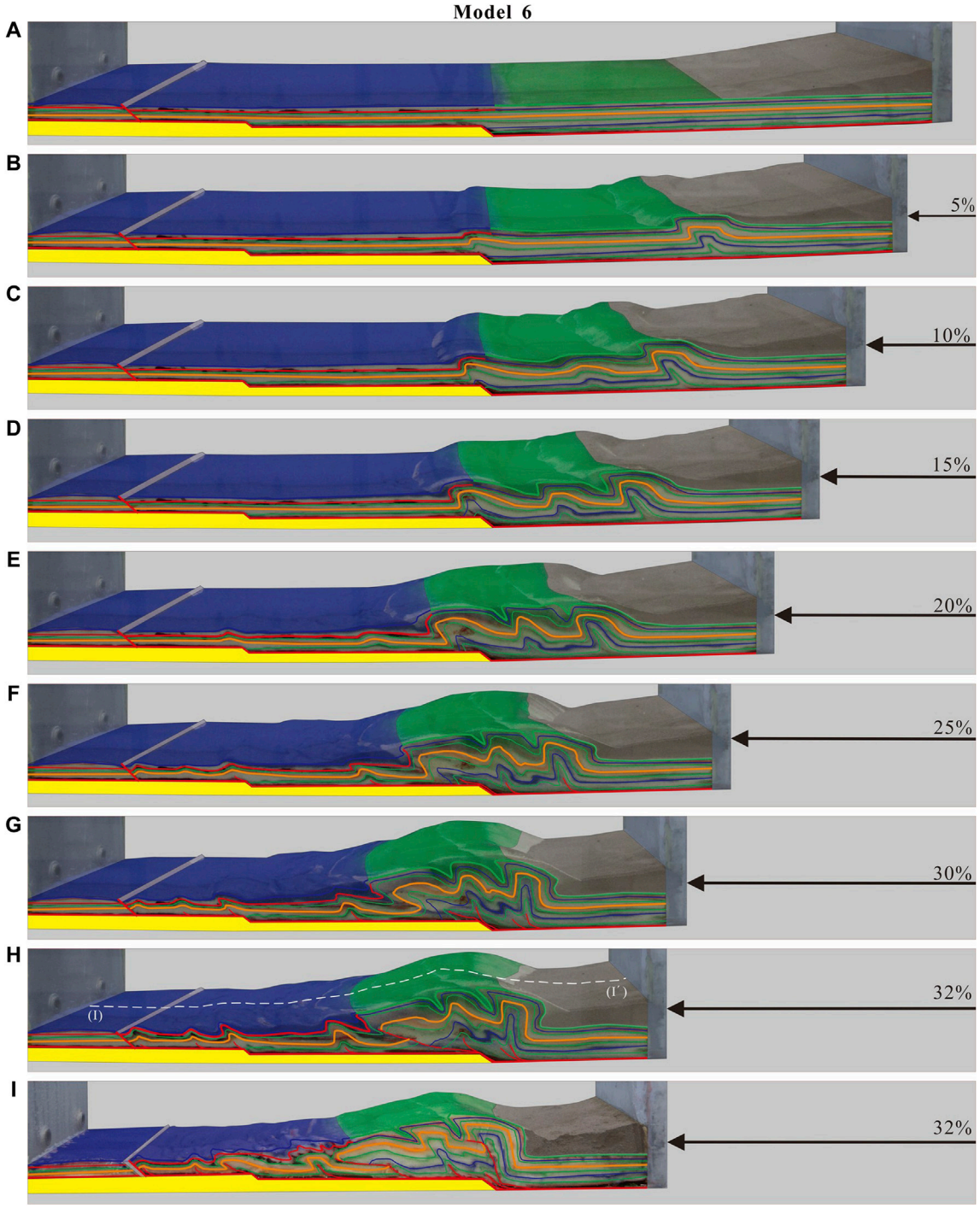

FIGURE 12 | Sequential deformation features of model-6.

upper slip fault in the trailing edge tectonic zone in model 5 absorbed more of the displacement, which may be the main reason for its shorter transmission distance compared with that in model 4. In the model containing two sets of slip layers, the positive retrograde fault propagating upward from the bottom slip layer was the main deformation mode, and its propagation mode was forward spreading. The fault broke through the quartz sand layer without breaking through the upper slip layer; so, the rock layer was mostly a retrograde fault under the upper slip layer, while it bent above to form back-slip folds.

Based on the deformation pattern of models 3–6, the folding of the microglass bead layer (non-ergodic layer) was mainly

controlled by bending flow deformation, and the material between the layers appeared to thicken or thin abnormally, forming two types of folding deformation patterns: 1) thin top and thick flank and 2) thick top and thin flank. When the quartz sand layer (dry layer) was subjected to extrusion fold deformation, it exhibited a bending and sliding fold pattern, and the thicknesses of the vertical layers were basically equal, i.e., the layers of the folds were basically in line with the concentric fold law. However, by changing the elevation height of the basement in the model, the cover layer with a larger thickness above the slip layer easily formed a septate fold. The ESFTB is controlled by boundary fractures, the crystalline basement in the lower crust, and the overlying Cambrian and Triassic slip layers. The foreshortening fault developed at the foremost edge of the model is similar in nature to the Huaying Mountain fault, and the location of the depth change of the slip layer in the model is comparable to that of the Qiyue Mountain fault and Dayong fault. When the model's shortening rate reached 25%, the deformation of the physical model began to accelerate. This stage corresponds to the tectonic deformation stage in the Yanshan period. This is consistent with the low-temperature thermal chronology data obtained in previous studies and the equilibrium section evidence, which indicate that during the Mesozoic, the strata in the study area experienced a rapid expansion of faults and a rapid increase in the fold amplitude (Mei et al., 2010; Li et al., 2011). The shortening rate of the Eastern Sichuan fold zone at the end of the experiment was about 32%, and the total shortening was about 140 km. The ESFTB developed from southeast to northwest in the order of snow peak uplift, slotted tectonic zone, slot-file transition zone, and Middle Sichuan weak deformation zone. By changing the boundary conditions of model 6, simulation results that were in general agreement with the geological prototype were finally obtained (**Figure 3B**). Similar to the natural geological structures, model 6 shows that the Western Hunan–Hubei domain is dominated by trough-like folds, while the Eastern Sichuan domain is dominated by high-steep anticlines.

5.2 Structural Characteristics of the Fold and Thrust Belt

The tectonic style of the study area is a typical folded-alluvial belt style, and the geomorphological features are extremely complex, which makes analyzing the tectonic style very difficult. The uplift of the landforms in western Hunan–Europe was large, while the landforms in Eastern Sichuan are low overall but are locally high and steep (**Figure 2D**). The tectonic style of the study area varies significantly from one tectonic unit to another. A large number of previous studies have shown that the overall tectonic characteristics are that the cover layer slipped and deformed above the basement. A large number of reverse faults were developing, and the cover fold slipping surface was mostly located in the Cambrian system above the Aurora system. The top interface of the basement was the deepest slip boundary, and the cover layer and the basement constituted a significant tectonic incompatibility. The main deformation was concentrated in the central tectonic layer (S-T), and the regional stress field and basement fracture control influenced the style of the deep and shallow tectonic assemblages in the study area, resulting in a certain degree of differences from east to west (Liu 1995; Ding et al., 2005; Mei et al., 2010). The tectonic zone in western Hunan–Europe is strongly deformed, and the basal Paleozoic strata have been uplifted up to the surface, forming a series of folds with a wide backward slope and a tight backward slope. The tectonic style is a typical basal-involved septal fold structure. The tectonic zone in Eastern Sichuan is steep and complex, but the stratigraphic deformation is weaker than that in western Hunan–Europe. Regarding the surface deposition in the Triassic and Jurassic systems, on the plane, the tectonic style is a septal fold structure with a wide and slow oblique and tight backward slope.

From the available seismic analysis results (**Figure 13**), the study area was influenced by the basement slip fault, which caused significant uplift and deformation of the tectonic layers, and the large pushover fault that developed at the back edge of the deformation allowed coordinated deformation. It cuts through all the tectonic layers and makes a certain degree of connection between them; so, the deformation characteristics of each tectonic layer tend to be consistent, while the deformation of the layers is different (Zhang 2019). In the vertical direction, the seismic profile exhibits obvious tectonic differentiation, and the general rule is that the upper tectonic layers are concentric equal-thickness folds, which are tectonically complete, tightly closed, high, steep, and large in scale. The fractures in the wings of the energetic rock folds in the central tectonic layers are very well developed, and the non-energetic layers located above and below them often underwent plastic flow and formed uncoordinated folds with thick wings and thin tops or thick tops and thin wings. The lower tectonic layer still experienced concentric and equal-thickness folding, and the structure is nearly symmetrical, gradually becoming shallower downward. In addition, the two flanking dip-axis faults often form a Y-shape and then disappear at the bottom of the crystalline basement (Li 2015).

Based on the results of the physical simulation experiments, it was concluded that large thrust faults developed at the deformed trailing edge of the study area only when there was a basement slip layer, and the slip layer underwent multiple transgressive uplift events from southeast to northwest. In the location where the basal slip layer was uplifted, rebound faults and anticlinal faults were more likely to develop, the formation mechanism of which was lateral and vertical upward flow of the basal slip layer under the extrusion stress. During the extrusion process, recoil faults easily formed between the adjacent slip layers in the vertical direction, leading to stepwise uplift of the basal slip layers, and the middle-superior tectonic layers were further developed on this basis. This phenomenon was also confirmed during the physical simulation experiments.

5.3 Deformation Evolution and Mechanisms

Regarding the analysis of the kinematic extension process of the East Sichuan fold-splash belt, considerable research has been carried out on this topic, and various models of the deformation extension genesis have been proposed (Liu 1995; Li et al., 2002; Yan et al., 2003; Hu et al., 2009; Ding et al., 2005; Ding et al., 2005;

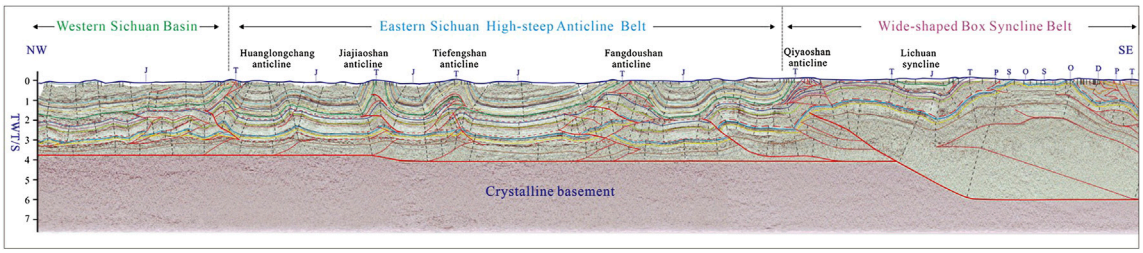

FIGURE 13 | Interpreted seismic section across the ESFB (modified after Zhang 2019).

Ding et al., 2008; Mei et al., 2010; Li et al., 2015; Yan et al., 2016; Gu et al., 2021). The genesis of the Eastern Sichuan fold-fault zone has been described by previous authors, and their results can be summarized as the following four main approaches: 1) the two backs and one break theory (Li et al., 2002); 2) the fault traction fold theory (Yan et al., 2003); 3) the external stress theory (Liu 1995); and 4) the cohesive difference and overburden pressure theory (Zhang 1997). According to Li et al. (2002), the study area has undergone a tectonic evolution process of early septal fold assemblage, a middle two backs and one break tectonic pattern, and finally late septal folding. When the rock layer was displaced upward along the bottom slip layer, an initial backslope with a sharp-edged tectonic style was formed due to traction. As the extrusion continued, the backslope further expanded to form a septal fold when the rock layers overlapped significantly at the fault slope. According to Zhang et al. (2019a), when the strata were buried at shallow depths, the interstratigraphic cohesion difference played a major role in controlling the folding. When the interstratigraphic cohesion difference was small, sagging folds formed. When the strata were buried deeper, the overlying stratigraphic pressure was the main controlling factor, and only septal folds formed.

To analyze the geodynamic origin of the arcuate belts, the following three main factors should be taken into consideration: first, the lithologic combination of the strata is indispensable in understanding the deformation of the geological structure. From the Aurignacian to the Middle Triassic, the study area developed and evolved into a passive continental margin basin due to intermittent intra-land rifting. From the Late Triassic to the Jurassic, the study area entered the foreland basin evolutionary stage due to the influence of the circumferential collisional orogeny, and the Sujiahe Formation was deposited in the Sichuan Basin (Li et al., 2002). During this period, more than 10,000 m of carbonate, paste rocks, sandstone, and mudstone were deposited in the Eastern Sichuan area. The soft and hard stratigraphic sequences were deposited in the Eastern Sichuan area (**Figure 4**). The difference in the interstratigraphic cohesion between the competent and non-competent layers and the high rheology of the slippage layers supplied the necessary stratigraphy and lithology for the formation of the Eastern Sichuan fold fault zone.

Second, the boundary conditions were also an important factor. The boundary geometry was an important controlling factor in the generation of the tectonic deformation style, and the results of this study show that the high, steep folded fault zone in Eastern Sichuan was affected by the pre-existing regional faults (the arc-shaped high-angle Qiyue Mountain Fault and Huaying Mountain Fault in the SW projection) (He and Zhou 2018; Wu et al., 2019), together with the step-like system composed of the slickensides and basement detachment surface. When the burial depth of the slip layer is shallow, the stratum forms a septal fold; when the burial depth of the slip layer increases, the stratum forms a septal groove fold.

Finally, the formation of the Eastern Sichuan fold-fault zone was inextricably linked to the evolution of the tectonic stress fields in the different geological periods. The complex structural style observed on the plane and in the profiles in the study area and the variable kinematic indicators are the result of the superposition of multiple periods of tectonic activity. 1) During the Garidonian–Haixi period, a series of cryptic fractures formed in Eastern Sichuan, which are basically consistent with the fold axis, and mainly underwent differential lifting and lowering movements in a tensional environment, forming a relatively gentle fold-combination style paleotectonic pattern of compartmentalized tectonics. 2) In the early stage of the Indo-Chinese movement, the fracturing activity strengthened, and the extrusion between the Pacific Plate and the Asian Plate along the western Pacific Ocean caused step-like differential uplift of the strata in Eastern Sichuan. At this time, the cover layer was deformed by extensional slip, with the weak Cambrian rock layer acting as the main slip layer, forming the prototype of the extrusion folding. 3) Entering the Yanshan period, further extrusion in the NW–SE direction caused the Mesozoic strata to expand and fold with increasing amplitude. 4) In the Xishan period, the Indian Ocean Plate collided with the Asian–European Plate and transformed the pre-existing NE-oriented fold belt into NNE-oriented spacer folds, and the inherited structures were transformed during this period. With the further strengthening of the extrusion stress of the circumferential massif, the regional differential uplift and denudation were strong, with an early uplift time, large uplift amplitude, and high denudation degree in the western Hunan–European region, exposing septal fold type folds. In Eastern Sichuan, the uplift occurred later, the uplift amplitude was smaller, and shallow separate folds were exposed.

5.4 Effects on the Construction of Karst Tunnels

The geological conditions in the study area are complex, and the construction of mountain tunnels often encounters

disadvantageous karst geological phenomena, especially karst surge water, which can affect the progress of the project in minor cases and cause loss of life and property in extreme cases (Xu, 2018). The constructed tunnel becomes a new groundwater drainage obstruction, changing the groundwater circulation path and causing a significant drop in the groundwater level, which destroys the equilibrium state of the groundwater environment and has negative effects on the geological environment, such as surface water point leakage, reservoir drought, and surface karst collapse (Gong 2010; Liu et al., 2015; Zhong 2018). Identifying the karst engineering hydrogeological conditions in the high steep backslope in Eastern Sichuan and the traffic corridor that can be passed through the planned tunnel is beneficial to achieving sustainable development of the economy and ecological environment in Eastern Sichuan.

The unique tectonic background and stratigraphic assemblage in the high and steep back-slope area in Eastern Sichuan control the direction of the groundwater runoff and the karst development. The development of karst landforms is closely related to the nature of the rocks, geological structures, and alternating conditions of the water circulation, which causes the karst landform assemblage to exhibit obvious spatial variation. In this study, we focused on two points: fold and fracture tectonics.

1) The karst development characteristics and distribution range of the folds are related to the sequence of the rock layers, the thickness of the soluble rocks, the degree of rock bending, the characteristics of the joint fracture development, and the water catchment. Under the special geological and tectonic background, the soluble rocks and non-soluble rocks in the study area are alternately exposed in the near-core part of the backslope in the form of strips. Usually, the tighter the axis of the backslope, the larger the scale of the accompanying longitudinal fissures, and the phenomenon of interlayer deficiency can even occur, which is conducive to the infiltration and flow of groundwater and the concentration of groundwater into the deep circulation. Thus, the karst development is, especially strong, and the surface is mostly developed along the longitudinal structural surface of the large-scale karst depressions in the form of beads; for example, the scale of the karst depressions in the northern Yangtze River region in the Guanyinxia backslope is more than 0.2 km^2. In contrast, the karst depressions developed in the core of the box-shaped backslope are dense but small in scale, and the groundwater circulation and dissolution are more dispersed. Thus, the scale of the karst depressions developed on the surface is smaller, such as the depressions developed in the north section of the Yulin River in the Mingyue Mountain backslope, but their areas are small, mostly <0.1 km^2. Regarding the asymmetric high steep backslope, the slow flanks usually have weak interlayer fissure development, and they often form small-scale troughs or bead-like karst depressions. The longitudinal fissures in the steeper flank are more developed, and the longitudinal fissures are conducive to the concentrated circulation and dissolution of the surface and groundwater. They often form a cascading dark river pipeline in this flank (e.g., the Zhongliang Mountain Dry Weantang Reservoir-Qingliangan Dark River Pipeline), and the transverse fissures provide a convenient way for the karst pipeline to break through the restriction imposed by the non-soluble rocks in the vertical direction. For example, the Huaying Mountain Green Water Cave Dark River connects the Feixianguan Formation with the karst groundwater of both the Feixianguan and Jialingjiang Formations, which makes the karst development characteristics and karst hydrogeological conditions complicated. Therefore, the steep flanks mostly develop long, continuous, large-scale karst troughs and valleys.
2) In general, the karst development in the fault zone decreases gradually as the tensor faults transition to compressional faults. Under the strong tectonic compressional effect, the associated faults are mainly compressional-torsional faults, and the fault zones are mostly closed and are characterized by vesiculation and water isolation. However, the influence of the compressional-torsional faults with developed joints and fissures increases as the fragmentation of the rock body, the water-richness, and the degree of karst development increase. For example, the 260-m burial depth of the Zhongliang Mountain Sheima Tunnel intersects the Baimiaozi reverse fault at a large angle on the western flank of the back-slope, and the fault fragmentation zone and influence zone have well-developed joint fissures and broken rock masses. After the excavation, water gushed into the entire section in the form of rain and fissure strands, and wide dissolution and pores were intensively developed. The fault fragmentation zone of the tensor fault had a large degree of fracturing, a high fissure rate, and a strong water-richness, and the karst activity mostly occurred along the fault zone. Under the effect of differential dissolution, many karst pipes and dark rivers were formed, such as the large-scale pearl-shaped waterfall caves developed along the N-S orthogonal fault in the Cataract Gorge on the north side of the Yangtze River on the backslope of the Guanyin Gorge. The influence of fault development on the groundwater distribution and karst development is manifested in the width of the different tectonic fault zones and structural surface development characteristics, and fracture displacement is another important factor affecting karst development. For example, the activity on the Baimiaozi reverse fault has led to the direct contact between the third section of the Feixianguan Group tuff and the Jialingjiang Group tuff, which are divided by the fourth section of the Feixianguan Group shale, and the originally relatively independent karst aquifers have established a unified hydraulic connection. This led to serious leakage of shallow karst water from the three sections of tuffs in the Feixianguan Group when the tunnel excavation process reached the tuffs of the Jialingjiang Group.
3) The high steep back-slope mountains are natural barriers to the east-west traffic corridors in the Eastern Sichuan area, seriously hindering the economic development of urban areas. Tunnels can be used to quickly traverse folded mountainous

areas, but the impact of trans-ridge tunnel construction on regional groundwater levels often induces serious geological disasters such as karst collapse, underground aquifer destruction, and surface water evacuation and drying, threatening the safe construction of tunnels and the local ecological and geological environment. For example, 300 karst collapses and about 110 drained wellsprings have occurred in the Zhongliang Mountain area (Wu et al., 2021). The karst collapses have mainly been concentrated in the low-lying karst trough valleys or karst depressions on the steeper backslope flank. Because the tension fissures are more developed, these zones are more conducive to the pooling of surface water and groundwater, and the alternating cycle of the groundwater level is more intense. The precondition for a collapse to occur is the existence of a karst fissure or cave system in the surface layer of bedrock at a certain depth below the ground. Targeted blocking and prevention measures can improve the prevention and control of karst collapse disasters and achieve better economic and social effects.

6 CONCLUSION

From the preceding analysis and the analog model experiments conducted in this study, we drew the following major conclusions:

1) The physical simulation experiments revealed that the lithology of the cover layer in the fold formation area should not be too soft or too hard in the deformation stage; otherwise, a series of foreshortening stacked tile recoil thrusting structures and recoil fault structures will form.
2) The different interstratigraphic cohesion between the competent and non-competent layers and the high rheology of the slip layers provide the necessary stratigraphic lithology for the formation of the Eastern Sichuan fold-fault zone. The multi-layered detachment slip structure is the fundamental reason for the formation of the fault-fold tectonic style in the study area.
3) The area where the basal detachment surface or the lower slip layer is uplifted is the location of the tectonic stress concentration, which is more likely to develop recoil faults.
4) The deformation of the ESFTB was controlled by a step-like system composed of the lower crustal crystalline basement detachment surface, regional boundary fractures, and the overlying Cambrian and Triassic slickensides. When the burial depth of the slip layer is shallow, the stratum forms septal folds.
5) The regional tectonic pattern generally exhibits the forward-spreading retrogradational thrusting and overlapping thin-skin structure style, with a complex structural style in the plane and profiles and variable kinematic indicators, which were caused by the superposition of multiple phases of tectonic activity.
6) The developed karst features are not conducive to the construction of the project tunnel in the area with a tightly closed backslope, fissures, and normal faults in the Eastern Sichuan fold and fault zone.

DATA AVAILABILITY STATEMENT

The raw data supporting the conclusion of this article will be made available by the authors, without undue reservation.

AUTHOR CONTRIBUTIONS

Y-SW, MX, and Y-NY contributed to the conception and design of the study. QX organized the database. CY performed the statistical analysis. Y-SW wrote the first draft of the manuscript. QX, BJ, CY, and HZ wrote sections of the manuscript. All authors contributed to manuscript revision and read and approved the submitted version.

FUNDING

This study was supported by the Natural Science Foundation of China's project under No. 42072283.

ACKNOWLEDGMENTS

We thank Professor Li Zhongquan from the School of Earth Sciences, Chengdu University of Technology, for the physical simulation experiment of the Key Laboratory of Tectonic Mineralization and Accumulation of the Ministry of Natural Resources. Dr. Ding Xiao's assistance during the experiment is appreciated. LetPub (www.letpub.com) is appreciated for its linguistic assistance during the preparation of this manuscript.

REFERENCES

Adrian, P. O. (2017). 'Thick-Skinned and Thin-Skinned Tectonics: A Global Perspective. *Geosciences* 7, 71. doi:10.3390/geosciences7030071

Bonini, M., Sani, F., and Antonielli, B. (2012). Basin Inversion and Contractional Reactivation of Inherited Normal Faults: A Review Based on Previous and New Experimental Models. *Tectonophysics* 522-523 (3), 55–88. doi:10.1016/j.tecto.2011.11.014

Boutoux, A., Bellahsen, N., Nanni, U., Pik, R., Verlaguet, A., Rolland, Y., et al. (2016). Thermal and Structural Evolution of the External Western Alps: Insights from (U-Th-Sm)/He Thermochronology and RSCM Thermometry in the Aiguilles Rouges/Mont Blanc Massifs. *Tectonophysics* 683, 109–123. doi:10.1016/j.tecto.2016.06.010

Brogi, A. (2008). Kinematics and Geometry of Miocene Low-Angle Detachments and Exhumation of the Metamorphic Units in the Hinterland of the Northern Apennines (Italy). *J. Struct. Geol.* 30, 2–20. doi:10.1016/j.jsg.2007.09.012

Buchanan, P. G., and Mcclay, K. R. (1991). Sandbox Experiments of Inverted Listric and Planar Fault Systems. *Tectonophysics* 188 (1–2), 97–115. doi:10.1016/0040-1951(91)90317-l

Charvet, J. (2013). The Neoproterozoic-Early Paleozoic Tectonic Evolution of the South China Block: An Overview. *J. Asian Earth Sci.* 74, 198–209. doi:10.1016/j.jseaes.2013.02.015

Chu, Y., Faure, M., Lin, W., and Wang, Q. (2012a). Early Mesozoic Tectonics of the South China Block: Insights from the Xuefengshan Intracontinental Orogen. *J. Asian Earth Sci.* 61, 199–220. doi:10.1016/j.jseaes.2012.09.029

Chu, Y., Lin, W., Faure, M., Wang, Q., and Ji, W. (2012b). Phanerozoic Tectonothermal Events of the Xuefengshan Belt, Central South China: Implications from UPb Age and LuHf Determinations of Granites. *Lithos* 150, 243–255. doi:10.1016/j.lithos.2012.04.005

Costa, E., and Vendeville, B. C. (2002). Experimental Insights on the Geometry and Kinematics of Fold-And-Thrust Belts above Weak, Viscous Evaporitic Décollement. *J. Struct. Geol.* 24, 1729–1739. doi:10.1016/s0191-8141(01)00169-9

Davis, D. M., and Engelder, T. (1985). The Role of Salt in Fold-And-Thrust Belts. *Tectonophysics* 119, 67–88. doi:10.1016/0040-1951(85)90033-2

Deng, Y., Zhang, Z., Badal, J., and Fan, W. (2014). 3-D Density Structure under South China Constrained by Seismic Velocity and Gravity Data. *Tectonophysics* 627, 159–170. doi:10.1016/j.tecto.2013.07.032

Ding, D., Guo, T., and Zhai, C. (2005). Knee-fold Structure in the Western Ezhou-Yudong Region[J]. *Pet. Exp. Geol.* 27 (03), 205–210. (In Chinese and English Abstract). doi:10.3969/j.issn.1001-6112.2005.03.001

Dong, Y., Zha, X., Fu, M., Zhang, Q., Yang, Z., and Zhang, Y. (2008). Characteristics of the Dabashan fold Thrust Nappe Structure at the Southern Margin of the Qinling,China. *Geol. Bull. China* 27 (9), 1493–1508. (In Chinese and English Abstract). doi:10.3969/j.issn.1671-2552.2008.09.011

Eisenstadt, G., and Sims, D. (2005). Evaluating Sand and Clay Models: Do Rheological Differences Matter? *J. Struct. Geol.* 27, 1399–1412.

Expósito, I., Balanyá, J. C., Crespo-Blanc, A., Díaz-Azpiroz, M., and Luján, M. (2012). Overthrust Shear Folding and Contrasting Deformation Styles in a Multiple Decollement Setting, Gibraltar Arc External Wedge. *Tectonophysics* 576-577, 86–98. doi:10.1016/j.tecto.2012.04.018

Faure, M., Lin, W., and Le Breton, N. (2001). Where Is the North China-South China Block Boundary in Eastern China? *Geol* 29, 119–122. doi:10.1130/0091-7613(2001)029<0119:witncs>2.0.co;2

Faure, M., Lin, W., Monié, P., and Meffre, S. (2008). Palaeozoic Collision between the North and South China Blocks, Triassic Intracontinental Tectonics, and the Problem of the Ultrahigh-Pressure Metamorphism. *Comptes Rendus Geosci.* 340, 139–150. doi:10.1016/j.crte.2007.10.007

Ghazian, R. K., and Buiter, S. J. H. (2014). Numerical Modelling of the Role of Salt in Continental Collision: An Application to the Southeast Zagros Fold-And-Thrust Belt. *Tectonophysics* 632, 96–110. doi:10.1016/j.tecto.2014.06.006

Gomes, C. J. S. (2013). Investigating New Materials in the Context of Analog-Physical Models. *J. Struct. Geol.* 46, 158–166.

Gong, R. (2010). Study on the Impact of Tunnel Construction on the Groundwater Environment of Septic Karst-Rich Backslope. *Environ. Sci. Pollut. Res. Int.* 28, 40203–40216. doi:10.1007/s11356-021-13919-1

Graveleau, F., and Dominguez, S. (2008). Analogue Modelling of the Interaction Between Tectonics, Erosion and Sedimentation in Foreland Thrust Belts. *Geoscience* 340, 324–333. doi:10.1016/j.crte.2008.01.005

Graveleau, F., Malavieille, J., and Dominguez, S. (2012). Experimental Modelling of Orogenic Wedges: A Review. *Tectonophysics* 538-540, 1–66. doi:10.1016/j.tecto.2012.01.027

Gu, Z., Wang, X., Nunns, A., Zhang, B., Jiang, H., Fu, L., et al. (2021). Structural Styles and Evolution of a Thin-Skinned Fold-And-Thrust Belt with Multiple Detachments in the Eastern Sichuan Basin, South China. *J. Struct. Geol.* 142, 104191. doi:10.1016/j.jsg.2020.104191

Hayes, M., and Hanks, C. L. (2008). Evolving Mechanical Stratigraphy during Detachment Folding. *J. Struct. Geol.* 30, 548–564. doi:10.1016/j.jsg.2008.01.006

He, W., and Zhou, J. (2018). 'Physical Simulation of the Characteristics and Formation Mechanism of the Southeast Sichuan Horsetail Fold Belt. *Earth Sci.* 43, 2133–2148. doi:10.3799/dqkx.2020.202

Hu, S., Zhu, G., and Liu, G. (2009). The Folding Time of the Eastern Sichuan Jura-Type Fold Belt: Evidence From Unconformity. *Geol. Rev.* 55 (1), 32–42. (In Chinese and English Abstract)

Huang, H., He, D., and Li, Y. (2019). Determination and Formation Mechanism of the Luzhou Paleo Southeatern Sichuan Basin. *Earth Sci. Front.* 26 (1), 102–120. doi:10.1016/j.ngib.2021.08.003

Hubbert, M. K. (1937). Theory of Scale Models as Applied to the Study of Geologic Structures. *Geol. Soc. Am. Bull.* 48, 1459–1520. doi:10.1130/gsab-48-1459

Jamison, W. R. (1992). Stress Spaces and Stress Paths. *J. Struct. Geol.* 14, 1111–1120. doi:10.1016/0191-8141(92)90063-3

Koyi, H. A., and Cotton, J. (2004). Experimental Insights on the Geometry and Kinematics of Fold-And-Thrust Belts above Weak, Viscous Evaporitic Décollement; a Discussion. *J. Struct. Geol.* 26, 2139–2141. doi:10.1016/j.jsg.2004.04.001

Krantz, R. W. (1991). Measurements of Friction Coefficients and Cohesion for Faulting and Fault Reactivation in Laboratory Models Using Sand and Sand Mixtures. *Tectonophys.* 188, 203–207.

Li, C., He, D., Sun, Y., He, J., and Jiang, Z. (2015). Structural Characteristic and Origin of Intra-continental Fold Belt in the Eastern Sichuan Basin, South China Block. *J. Asian Earth Sci.* 111, 206–221. doi:10.1016/j.jseaes.2015.07.027

Li, F. (2015). *Study on the Seismic Hazard of Isolated Back-Slope Structures in Chongqing*. China: Ph.D., Institute of Geology.

Li, X.-H., Li, W.-X., Li, Z.-X., Lo, C.-H., Wang, J., Ye, M.-F., et al. (2009). Amalgamation between the Yangtze and Cathaysia Blocks in South China: Constraints from SHRIMP U-Pb Zircon Ages, Geochemistry and Nd-Hf Isotopes of the Shuangxiwu Volcanic Rocks. *Precambrian Res.* 174, 117–128. doi:10.1016/j.precamres.2009.07.004

Li, Z., Ran, L., Chen, Z., Lu, Z., and Duan, X. (2002). 'Geological Model and Gas-Bearing Analysis of High Steep Tectonic Genesis in East Sichuan. *J. Chengdu Inst. Technol.* 1, 605–609. doi:10.1016/j.engeos.2020.06.005

Li, Z. X. (2007). Formation of the 1300-km-wide Intracontinental Orogen and Postorogenic Magmatic Province in Mesozoic South China: A Flat-Slab Subduction Model. *Geology*, 35 179–182. doi:10.1130/G23193A.1

Li, S., Li, J., and Zhou, Y. (2011). Evidence of Fission Traces for the Middle Cenozoic Tectonic Uplift in the Southeastern Margin of the Sichuan Basin. *J. Petrology Mineralogy* 30 (2), 225–233. (In Chinese and English Abstract). doi:10.3969/j.issn.1000-6524.2011.02.007

Liu, D., Yang, L. Z., and Yu, S. U. J. (2015). Ecological and Environmental Problems and Effects of Drainage in the Huayin Mountain Tunnel [J]. *J. Southwest Jiaot. Univ.* 36 (3), 308–313. (In Chinese and English Abstract). doi:10.3969/j.issn.0258-2724.2001.03.021

Liu, S. (1995). The Thin-Skinned Tectonic Model of Eastern Sichuan[J]. *Sichuan J. Geol.* 15 (4), 264–267. (In Chinese and English Abstract).

Lu, G., Zhao, L., Zheng, T., Kaus, B. J. P., and Kaus, P. (2014). Strong Intracontinental Lithospheric Deformation in South China: Implications from Seismic Observations and Geodynamic Modeling. *J. Asian Earth Sci.* 86, 106–116. doi:10.1016/j.jseaes.2013.08.020

Malz, A., Madritsch, H., Meier, B., and Kley, J. (2016). An Unusual Triangle Zone in the External Northern Alpine Foreland (Switzerland): Structural Inheritance, Kinematics and Implications for the Development of the Adjacent Jura Fold-And-Thrust Belt. *Tectonophysics* 670, 127–143. doi:10.1016/j.tecto.2015.12.025

Massoli, D., Koyi, H. A., and Barchi, M. R. (2006). Structural Evolution of a Fold and Thrust Belt Generated by Multiple Décollements: Analogue Models and Natural Examples from the Northern Apennines (Italy). *J. Struct. Geol.* 28, 185–199. doi:10.1016/j.jsg.2005.11.002

Mei, L., Liu, Z., and Tang, J. (2010). Progressive Intra-terranean Extensional Deformation in the Xiang-Exi-Eastern Sichuan Mesozoic: Evidence from Fission Traces and Equilibrium Profiles. *Earth Sci.* 35 (2), 161–174. (In Chinese and English Abstract).

Meng, Q., and Hodgetts, D. (2019). Structural Styles and Decoupling in Stratigraphic Sequences with Double Décollements during Thin-Skinned Contractional Tectonics: Insights from Numerical Modelling. *J. Struct. Geol.* 127, 103862. doi:10.1016/j.jsg.2019.103862

Mount, V. S. (2014). Structural Style of the Appalachian Plateau Fold Belt, North-Central Pennsylvania. *J. Struct. Geol.* 69, 284–303. doi:10.1016/j.jsg.2014.04.005

Mulugeta, G., and Koyi, H. (1992). Episodic Accretion and Strain Partitioning in a Model Sand Wedge. *Tectonophysics* 202, 319–333. doi:10.1016/0040-1951(92)90117-o

Oner, Z., and Dilek, Y. (2013). Fault Kinematics in Supradetachment Basin Formation, Menderes Core Complex of Western Turkey. *Tectonophysics* 608, 1394–1412. doi:10.1016/j.tecto.2013.06.003

Panien, M., Schreurs, G., and Pfiffner, A. A. (2006). Mechanical Behaviour of Granular Materials Used in Analogue Modelling: Insights from Grain Characterisation, Ring-Shear Tests and Analogue Experiments. *J. Struct. Geol.* 28, 1710–1724. doi:10.1016/j.jsg.2006.05.004

Rameil, N. (2008). Early Diagenetic Dolomitization and Dedolomitization of Late Jurassic and Earliest Cretaceous Platform Carbonates: A Case Study from the

Jura Mountains (NW Switzerland, E France). *Sediment. Geol.* 212, 70–85. doi:10.1016/j.sedgeo.2008.10.004

Reiter, K., Kukowski, N., and Ratschbacher, L. (2011). The Interaction of Two Indenters Inanalogue Experiments and Implications for Curved Fold-and-Thrust Belts. *Earth Planet. Sci. Lett.* 302, 132–146. doi:10.1016/j.epsl.2010.12.002

Rich, J. L. (1934). 'Mechanics of Low-Angle Overthrust Faulting as Illustrated by Cumberland Thrust Block, Virginia, Kentucky, and Tennessee. *AAPG Bull.* 18, 1584–1596. doi:10.1306/3d932c94-16b1-11d7-8645000102c1865d

Richardson, N. J., Densmore, A. L., and Seward, D. (2008). Extraordinary Denudation in the Sichuan Basin: Insights from Low-Temperature Thermochronology Adjacent to the Eastern Margin of the Tibetan Plateau. *J. Geophys. Res.* 113 (B4), 1–23. doi:10.1029/2006JB004739

Rossetti, F., Faccenna, C., Ranalli, G., and Storti, F. (2000). 'Convergence Rate-dependent Growth of Experimental Viscous Orogenic Wedges. *Earth Planet. Sci. Lett.* 178, 367–372. doi:10.1016/S0012-821X(00)00082-0

Santolaria, P., Vendeville, B. C., Graveleau, F., Soto, R., and Casas-Sainz, A. (2015). Double Evaporitic Décollements: Influence of Pinch-Out Overlapping in Experimental Thrust Wedges. *J. Struct. Geol.* 76, 35–51. doi:10.1016/j.jsg.2015.04.002

Shen, C. B., Mei, L. F., and Xu, S. H. (2009). 'Fission Track Dating of Mesozoic Sandstones and its Tectonic Significance in the Eastern Sichuan Basin, China. *Radiat. Meas.* 44, 945–949. doi:10.1016/j.radmeas.2009.10.001

Shu, L. S., Zhou, X. M., Deng, P., Wang, B., Jiang, S. Y., Yu, J. H., et al. (2009). 'Mesozoic Tectonic Evolution of the Southeast China Block: New Insights from Basin Analysis. *J. Asian Earth Sci.* 34, 376–391. doi:10.1016/j.jseaes.2008.06.004

Souloumiac, P., Maillot, B., and Leroy, Y. M. (2012). Bias Due to Side Wall Friction in Sand Box Experiments. *J. Struct. Geol.* 35, 90–101. doi:10.1016/j.jsg.2011.11.002

Tang, L., and Cui, M. (2012). Structural Deformation and Fluid Flow from East Sichuan to the Northwestern Periphery of the Xuefeng Uplift, China. *Petroleum Sci.* 9, 429–435. doi:10.1007/s12182-012-0226-5

Tavani, S., and Cifelli, F. (2010). Deformation Pattern Analysis and Tectonic Implications of a Décollement Level within the Central Apennines (Italy). *Geol. J.* 45, 582–596. doi:10.1002/gj.1198

Vendeville, B. C. (2007). "The 3-D Nature of Stress Fields in Physical Experiments and its Impact on Models Overall Evolution," in *European Geosciences Union General Assembly, 15e20 April 2007* (Vienna, Austria: EGU2007-A-02960).

Wang, P., Liu, S., and Gao, X. (2012a). AFT Record of Three-Dimensional Tectonic Extension in the Eastern Sichuan Arc. *J. Geophys.* 55 (5), 1662–1673. (In Chinese and English Abstract). doi:10.6038/j.issn.0001-5733.2012.05.023

Wang, W., Zhou, M. F., Yan, D. P., and Li, J. W. (2012b). Depositional Age, Provenance, and Tectonic Setting of the Neoproterozoic Sibao Group, Southeastern Yangtze Block, South China. *Precambrian Res.* 192-195, 107–124. doi:10.1016/j.precamres.2011.10.010

Wang, C. Y., Cheng, X. G., Chen, H. L., Ding, W. W., Lin, X. B., Wu, L., et al. (2016). The Effect of Foreland Palaeo-Up Lift on Deformation Mechanism in the Wupoer Fold and Thrust Belt, NE Pamir: Constraints From Analogue Modelling. *J. Geodyn.* 100, 115–129.

Wang, Y., Zhang, Y., Fan, W., and Peng, T. (2005). Structural Signatures and 40Ar/39Ar Geochronology of the Indosinian Xuefengshan Tectonic Belt, South China Block. *J. Struct. Geol.* 27, 985–998. doi:10.1016/j.jsg.2005.04.004

Woodward, N. B. (1999). Competitive Macroscopic Deformation Processes. *J. Struct. Geol.* 21, 1209–1218.

Wu, H., Qiu, N., Chang, J., Zhang, J., and Wang, Y. (2019). 'Physical Simulation of the Formation of Multiple Sets of Slip-Layer Folded Tectonic Zones in East Sichuan. *Earth Sci.* 44, 784–797. (In Chinese and English Abstract). doi:10.3799/dqkx.2018.109

Wu, Y. B., Yin, R. C., Lei, M. T., Dai, J. L., Jia, L., Pan, Z. Y., et al. (2021). Triggering Factors and Prevention-Control Countermeasures of Karst Collapses Caused by Tunnel Construction in the Zhongliangshan Area, Chongqing. China. *CARSOLOGICA Sin.* 40 (2), 246–252. doi:10.11932/karst20210204

Xu, Z. (2018). *Complex Karst Tunnel Surge Water Evolution Mechanism and Comprehensive Disaster Prevention and Control Research*. Chengdu University of Technology.

Yan, D., Xu, Y., and Dong, Z. (2016). Fault-related Fold Styles and Progressions in Fold-thrust Belts: Insights from Sandbox Modeling. *J. Geophys. Res. Solid Earth* 121 (3), 2086–2111. doi:10.1002/2015JB012397

Yan, D., Zhou, M., and Song, H. (2003). Origin and Tectonic Significance of a Mesozoic Multi-Layer Over-thrust System within the Yangtze Block (South China). *Tectonophysics*, 361, 239–254. doi:10.1016/S0040-1951(02)00646-7

Zanon, M. L., and Janette Souza Gomes, C. (2019). Sandbox Models of Fault-Bend Folding: A New Investigation with a Pre-existing Fault Ramp. *J. Struct. Geol.* 127, 103864. doi:10.1016/j.jsg.2019.103864

Zhang, K. J. (1997). North and South China Collision along the Eastern and Southern North China Margins. *Tectonophysics* 270, 145–156.

Zhang, X., Shan, Y., Nie, C., and Ni, Y. (2013). 'Numerical Simulation of the Mesozoic East Sichuan Fold Belt: Influence of Slip Zone Depth on Platform Cover Fold Patterns. *Geotect. Metallogeny* 37, 622–632. (In Chinese and English Abstract). doi:10.16539/j.ddgzyckx.2013.04.014

Zhang, X. L. (2019). *Tectonic Evolution and Genesis Mechanism of the West-East Eurasian Region*. Beijing: China University of Geosciences.

Zhang, Y. H., Cao, H. W., Hollis, S. P., Tang, L., Xu, M., Jiang, J. S., et al. (2019a). Geochronology, Geochemistry and Sr-Nd-Pb-Hf Isotopes of the Early Paleogene Gabbro and Granite from Central Lhasa, Southern Tibet: Petrogenesis and Tectonic Implications. *Int. Geol. Rev.* 61 (7), 868–894. doi:10.1080/00206814.2018.1476187

Zhang, Y. H., Dai, Y. S., Wang, Y., Huang, X. Y., and Pei, Q. M. (2021a). Hydrochemistry, Quality and Potential Health Risk Appraisal of Nitrate Enriched Groundwater in the Nanchong Area, Southwestern China. *Sci. Total Environ.* 784, 147186. doi:10.1016/j.scitotenv.2021.147186

Zhang, Y. H., He, Z. H., Tian, H. H., Huang, X., Zhang, Z. X., Liu, Y., et al. (2021b). Hydrochemistry Appraisal, Quality Assessment and Health Risk Evaluation of Shallow Groundwater in the Mianyang Area of Sichuan Basin, Southwestern China. *Environ. Earth Sci.* 80 (17), 576. doi:10.1007/s12665-021-09894-y

Zhang, Y. H., Li, X., Luo, M., Wei, C. L., Huang, X., Xiao, Y., et al. (2021c). Hydrochemistry and Entropy-Based Groundwater Quality Assessment in the Suining Area, Southwestern China. *J. Chem.* 559, 1–11. doi:10.1155/2021/5591892

Zhang, Y. H., Wang, Y. S., Wang, W. S., Liu, J., and Yuan, L. L. (2019b). Zircon U-Pb-Hf Isotopes and Mineral Chemistry of Early Cretaceous Granodiorite in the Lunggar Iron Deposit in Central Lhasa, Tibet Y, China. *J. Central South Univ.* 12, 3457–3469. doi:10.1007/s11771-019-4266-5

Zhao, D. (2017). *Tectonic Geometry and Kinematics of the Eastern Margin of the Sichuan Basin*. Beijing: China University of Geosciences.

Zhong, L. (2018). *'Study on the Spatial Differentiation Characteristics of Karst and the Construction of Evaluation System in the High Steep Backslope Area of East Sichuan*. Ph. D., Chengdu: Chengdu University of Technology.

Zhou, J., Xu, F., and Chunguang, W. (2007). Shortening of Analogue Models with Contractive Substrata: Insights into the Origin of Purely Landward-Vergent Thrusting Wedge along the Cascadia Subduction Zone and the Deformation Evolution of Himalayan-Tibetan Orogen. *Earth Planet. Sci. Lett.* 260 (1), 313–327. doi:10.1016/j.epsl.2007.05.048

Zou, H. (2011). *Characteristics of the Cambrian Gypsum-salt Rocks in Sichuan Basin*. MA: Chengdu University of Technology.

Zou, Y., Duan, J., Zhao, Y., Zhang, X., and Li, Z. (2015). 'Tectonic Features and Their Evolution in the High Steep Fault Zone of East Sichuan. *J. Geol.*, 558 2046–2052. doi:10.1007/s13202-016-0305-z

Conflict of Interest: Author HZ was employed by Sichuan Metallurgical Geological Survey and Design Group Co. Ltd.

The remaining authors declare that the research was conducted in the absence of any commercial or financial relationships that could be construed as a potential conflict of interest.